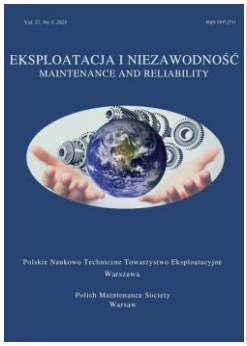

Eksploatacja i Niezawodnosc – Maintenance and Reliability
Volume 27 (2025), Issue 3
journal homepage: http://www.ein.org.pl

Article citation info:
Jin C, Yang T, Xu W, Qian Y, Huang J, An Evaluation on the Time-Dependent Reliability of Reinforced Concrete Structures Considering Non-Stationary Resistance Degradation: A Comprehensive Gamma Process-Based Approach, Eksploatacja i Niezawodnosc – Maintenance and Reliability 2025: 27(3) http://doi.org/10.17531/ein/200284

An Evaluation on the Time-Dependent Reliability of Reinforced Concrete Structures Considering Non-Stationary Resistance Degradation: A Comprehensive Gamma Process-Based Approach

Indexed by: Web of Science Group

Conghe Jin [a, *], Tao Yang [b], Wangxi Xu [c], Yongjiu Qian [c], Junhao Huang [d]

[a] School of Architecture and Civil Engineering, Xihua University, China
[b] Sichuan Provincial Geological Environment Survey and Research Center, China
[c] School of Civil Engineering, Southwest Jiaotong University, China
[d] Chengdu Municipal Transportation Bureau, China

Highlights

- Bridge resistance deteriorates non-stationarily over time, affecting safety.
- Load frequency and intensity growth impact time-dependent reliability.
- Gamma process models non-stationary degradation, validated by FE experiment.
- Two reliability equations developed based on Gamma process and load growth.
- Load intensity and non-stationary degradation are primary contributors to safety decline.

Abstract

Bridge resistance deteriorates over time, impacting safety and time-dependent reliability due to non-stationary degradation and increasing load frequency and intensity. This paper investigates the reliability of reinforced concrete structures, focusing on these factors. A Gamma process models the non-stationary degradation of bridge resistance, validated through a finite element experiment with a simply supported RC beam, where tensile steel reinforcements were reduced to simulate deterioration. Two time-dependent reliability equations were derived from the Gamma process and verified via Monte Carlo Simulation. Results show that the sensitivity of load intensity growth, frequency growth, non-stationarity degradation of resistance and environmental affection occupies 56.1%, 0.03%, 40.5% and 3.37%, respectively. Load intensity growth declines the safety of aging structures most, while the non-stationarity of resistance degradation should be given extra attention, as the analysis did not set expectations for its growth.

Keywords
gamma process, non-stationary degradation, RC beam, reinforcement corrosion, time-dependent reliability

1. Introduction

Over time, due to factors such as rebar corrosion, concrete deterioration caused by harsh environmental conditions, increased expected loads, and revisions to design guidelines, many RC structures fail to meet safety and usability requirements. [1].

In particular, bridges constructed during the 1980s and 1990s have experienced widespread issues related to aging, reinforcement corrosion, fatigue, and concrete cracking. These problems are exacerbated by the fact that designers during that period did not adequately account for the rapid increase in load intensity and frequency. Consequently, the service life of these bridges has been consumed at a much faster rate than anticipated, leading to numerous maintenance and repair challenges that have become an increasingly significant concern for engineers [2,3]. Modern engineering theory generally holds that addressing the problems of aging infrastructure requires not

(*) Corresponding author.
E-mail addresses: C. Jin (ORCID: 0000-0001-9108-2344) conghejin@163.com, T. Yang (ORCID: 0000-0001-9779-3868) 1029193228@qq.com, W. Xu (ORCID: 0000-0003-4347-8242) wxxu2018@sina.com, Y. Qian (ORCID: 0009-0006-7687-4267) yjqian@sina.com, J. Huang (ORCID: 0009-0003-4624-7535) hjhbridge@163.com

only targeted maintenance and retrofitting efforts but also a forward-looking design and construction approach that considers current and future conditions. As a result, the scientific management of such systems has become a key focus for engineers and policymakers alike, aiming to extend the service life of these structures while ensuring their safety and reliability [4].

As infrastructure continues to age, the degradation of performance and safety of existing structures has become an increasingly significant concern for engineers. Various factors, including material aging, adverse environmental conditions, and complex loading scenarios, contribute to the gradual decline in structural safety over time. For example, in the United States, approximately 56,000 bridges, or 9.1% of the total, were identified as structurally deficient as of 2017. Addressing the safety concerns of such aging structures necessitates substantial financial and material resources [5].

During the service life of reinforced concrete (RC) bridges, steel reinforcements are subjected to environmental erosion and live load effects, which, when combined with inadequate management and improper maintenance, lead to a gradual decline in resistance and durability. The corrosion of tensile steel reinforcements is the primary cause of functional deterioration in RC beams [6]. Corrosion reduces the effective cross-sectional area of the steel, and the resulting corrosion products cause spalling of the bonding layer in the reinforced concrete. This spalling weakens the bonding mechanism, diminishing the synergistic performance of the beam [7].

Furthermore, reinforcements that are subjected to frequent load effects are more susceptible to fatigue-induced bending and fracture, which compromises the stability and safety of the entire bridge structure. The impact of steel corrosion and fatigue on the bearing capacity of flexural RC components is significantly greater than on other structural capacities, underscoring the critical importance of addressing these issues to maintain the integrity and safety of RC bridges [8].

In response to these challenges, the reliability of civil-engineering structures is receiving more attention, as it helps decrease in-service uncertainties and serves as the economic basis for maintenance and repair. The safety assessment of aging structures is increasingly guided by structural reliability, which considers both the resistance of the structure and the loads it must bear. By continuously monitoring the condition of structures and evaluating their ability to withstand various loads, engineers can implement targeted maintenance strategies based on these assessments [2,9,10].

Structural resistance prediction plays a crucial role in reliability assessment, enabling engineers to forecast how a structure will perform under different conditions. This proactive approach helps anticipate potential failures, optimize maintenance efforts, and ultimately enhance safety while reducing costs and minimizing environmental impacts [11]. Impact of fatigue damage accumulation on prestressed concrete (PC) bridges and structures, emphasizing the combined effects of cyclic vehicle loading and environmental corrosion has been studied by numerous researchers [12–16]. As the literature review indicates, simply supported reinforced concrete (RC) bridges have been widely analyzed in reliability studies due to their direct stress-strain relationship, aging-induced degradation, and widespread application. These bridges are a common focus in reliability assessments because their straightforward structural behavior allows for more precise modeling of deterioration processes and performance under various conditions. This focus has made them a key area of study in addressing the reliability and maintenance challenges associated with aging infrastructure [17,18].Probabilistic-based reliability analysis is valuable because it explicitly accounts for uncertainty and provides a quantitative framework to assess whether a structure can withstand significant load processes during its remaining service life. This approach allows engineers to better predict the likelihood of structural failure and make informed decisions about maintenance, repair, and resource allocation, ultimately enhancing the safety and longevity of the infrastructure [19].

Matteo et al. [20] explored the reliability of the reinforced concrete (RC) Reactor Building (RB), which serves as the ultimate barrier against radioactive contamination from a Nuclear Power Plant (NPP). Traditional Probabilistic Risk Assessment (PRA)-Level 2 models do not account for the aging and degradation of the RB. In this study, the authors adopted a time-dependent reliability approach that explicitly models the effects of aging and degradation on the RB's resistance to accidental stresses and its failure probability. They developed a Finite Element Model (FEM) of the RC coupled with

a degradation model to update risk measures such as the Large Early Release Frequency (LERF) over time. A case study involving an internal overpressure due to a hydrogen explosion was used to demonstrate the methodology.Capacci and Biondini [21] presented a probabilistic framework for assessing the life-cycle seismic resilience of aging bridges and road networks, considering infrastructure upgrades. The framework accounts for uncertainties in bridge damage due to deterioration and the restoration speed of the overall system. It evaluates time-variant bridge fragilities and damage probabilities across different earthquake scenarios, incorporating traffic analyses to assess network functionality and resilience. The study also explored the impact of structural deterioration, seismic damage, and repair actions on traffic restrictions. Applied to reinforced concrete bridges and simple road networks, the framework demonstrated its effectiveness in quantifying deterioration's negative effects and the positive impact of infrastructure upgrades, such as adding road segments to improve network connectivity and resilience.Guo et al. developed a novel computational framework to assess the time-dependent reliability of reinforced concrete (RC) beams under marine atmospheric environments. This framework incorporates a comprehensive life-cycle performance assessment model that accounts for climate change, two-dimensional chloride transport, coupling effects, corrosion non-uniformity, and the nonlinear behavior of RC beams. Validated by experimental studies, the framework establishes performance functions for different failure modes and captures time-dependent probabilistic information using the probability density function-informed method (PDFM). The method's accuracy and efficiency were demonstrated through illustrative cases and validated by traditional Monte Carlo Simulation (MCS), showing its feasibility for the life-cycle design and maintenance of RC structures.Ben Seghier et al. [22] explored the use of an improved structural reliability method, specifically the three-term conjugate map (TCM) based on the first-order reliability method (FORM), for assessing the multi-state failure of corroded reinforced concrete (RC) beams. The study focused on the impact of uniform and pitting corrosion on the reliability of RC beams, considering brittle fracture due to pit-to-crack transition probability. The TCM method was validated against other well-known FORM formulations. Time-dependent reliability analyses were performed to evaluate the influence of parameters such as nominal bar diameter, corrosion initiation rate, and external loads on the failure probability of corroded beams. The results demonstrated that the TCM method outperformed other reliability-based methods in predicting the safety of RC beams under corrosion-induced deterioration. When the state of the studied system depends on its health condition at any given time, the concept of time-dependent reliability emerges. It considers allows for a more dynamic and realistic assessment of a system's performance throughout its service life, enabling better prediction of potential failures and more effective maintenance planning [23]. Earlier attempts by Mori and Ellingwood laid the foundation for the fundamental framework of time-dependent reliability, where the failure criterion for time-aging structures is defined as the first outcrossing occurrence. This concept identifies failure as the moment when the system's response first exceeds a critical threshold, considering the cumulative effects of aging and other time-related factors. Their work provided a basis for understanding and analyzing the reliability of structures over time, emphasizing the importance of tracking the progressive degradation of structural capacity and its impact on overall performance [24–26]. In their framework, Mori and Ellingwood also addressed the uncertainty associated with the stochastic degradation process in reliability analysis. By incorporating the randomness inherent in material degradation and environmental influences, their approach provides a more comprehensive understanding of how these uncertainties affect the time-dependent reliability of aging structures. This allows for more accurate predictions of structural performance and failure, ultimately leading to better-informed decisions regarding maintenance and risk management throughout the structure's life cycle. and the uncertainty associated with the stochastic degradation process has been addressed in the reliability analysis [27].

Among the various uncertainty modeling tools, the Gamma process is particularly useful when system degradation follows a continuous monotonic trend. The Gamma process is a stochastic process with independent, non-negative increments that follow a gamma distribution with a consistent scale parameter, which is considered one of the most appropriate processes for modeling the damage associated with the

cumulative degradation of a system and predicting the deterioration of structures, such as reinforcement corrosion and concrete cracking [28-30]. Unlike the Compound Poisson process, which has a finite number of jumps in finite time intervals, the Gamma process allows for an infinite number of small jumps, making it ideal for modeling gradual, continuous damage or degradation over time [31]. This process is favored for its ability to model gradual, irreversible deterioration over time, and its mathematical computations are relatively tractable, making it a practical choice for reliability analysis. It allows for the prediction of future degradation levels and the assessment of a structure's remaining useful life, enabling engineers to make informed decisions about maintenance and repair strategies [32-34]Noortwijk and Pandey [35] present a stochastic gamma process model to address both population (sampling) and temporal variability in degradation processes, which generally increase the probability of failure as structures age. Li [36] described the non-stationary degradation of structural resistance using the Gamma process. Jia and Wu [37] proposed an analyzing method for structures under non-stationary random seismic excitations, considering the combined effects of extreme values, where the extreme value distribution is established using the Gamma mixture model. D. Kuizo et al. [30] used the Gompertz cumulative hazard function instead of the linear function to propose a modification of the gamma process to predict system remaining useful life (RUL) with time-dependent degradation process and non-Gaussian random variables. Others [38,39] combined the non-monotonic characteristic of Gamma process with the memoryless property of Markov processes to develop mathematical models for capturing dynamic characteristics or assessing RUL of the structural systems. The previous works provide sufficient valuable references for this paper's use of the Gamma process to establish the cumulative damage of bridge resistance, because it can capture the temporal variability in the evolution of degradation. Therefore, the paper outlines two methods for estimating the parameters of the gamma process, making it more applicable to practical engineering scenarios.

Due to the inevitable discrepancies between the actual state of engineering structures and subjective measurements, the non-stationarity of structural resistance degradation with a non-monotonic trend has become a significant concern. This non-stationary degradation characteristic can have underestimated effects on structural reliability, making it essential to model and verify these behaviors through experimentation.

Additionally, when both the frequency and intensity of loads contribute to structural reliability concerns, it is crucial to determine which factor primarily drives the increase in structural failure probability through sensitivity analysis. This analysis helps to assess the relative impact of these factors, allowing for a more informed discussion on the degree of threat posed by congestion or the growth of vehicle axle loads to bridge safety. Understanding these dynamics is vital for developing effective strategies to mitigate risks and enhance the reliability of aging infrastructure.

1.1. Research gaps in the literature

The research gaps identified in the literature are:

1. **Rapid Load Increases:** Lack of strategies to address the unanticipated load increases on aging bridges.
2. **Time-Dependent Reliability:** Need for models that account for material degradation and varying conditions over time.
3. **Non-Stationary Degradation:** Insufficient modeling and verification of non-monotonic degradation in structural assessments.
4. **Sensitivity Analysis:** Need to determine whether load frequency or intensity is the main driver of failure.
5. **Experimental Validation:** Limited empirical data to support theoretical models, particularly for non-monotonic degradation.

1.2. Contributions of research

The contributions of this work are as follows:

1. **Development of a Non-Stationary Degradation Model:** This work establishes a non-stationary degradation model for bridge resistance that accounts for a non-monotonic trend in structural degradation. The model is thoroughly explained and validated through a carefully designed experiment, ensuring its accuracy and relevance to real-world scenarios.
2. **Formulation of Time-Dependent Reliability Equations:** Two time-dependent reliability equations are proposed based on the Gamma process. These equations incorporate the effects of non-stationary

resistance degradation, as well as variations in vehicle load intensity and frequency, providing a more comprehensive framework for assessing the reliability of aging bridges.

3. **Sensitivity Analysis for Safety Performance:** A sensitivity analysis is conducted to quantitatively evaluate the impact of different factors on bridge safety performance. This analysis helps identify the primary contributors to structural failure probability, facilitating a deeper understanding of the threats posed by congestion and increased vehicle axle loads to bridge safety.

2. Resistance degradation analysis of RC bridge

RC bridges face corrosion from environmental erosion and live loads, leading to reduced resistance and durability. Corrosion diminishes the steel's cross-sectional area, weakens the bond, and increases fatigue, compromising the bridge's stability and safety, particularly in flexural components. The corrosion of steel reinforcement in RC structures is complex. Initially, the concrete's protective layer mitigates damage, with iron oxide friction compensating for performance loss. Over time, rust expansion cracks the protective layer, accelerating corrosion, especially with chloride exposure. As corrosion progresses, internal force redistribution offers temporary ductility, delaying bearing capacity loss. However, ongoing corrosion ultimately compromises the structure's long-term durability and safety [40].

Bai et al. [1] conducted an analysis of ultimate bearing capacity of simply supported RC rectangular beams reinforced with U-shaped CFRP strips wrapped at both ends and FRP reinforcing in the tensile zone. The results indicated that there are small periods during the irreversible degradation process of the RC beams where the resistance does not decrease but rather increases since the decreases of deflection and reinforcement strain of the beam with the increase of loading were observed. The coexistence of accelerating corrosion and decelerating ductility leads to a non-stationary resistance degradation process in RC components, characterized by a "drop-balance-drop" trajectory. This non-stationary behavior results in fluctuations when compared to the standard degradation model $R_0 \cdot g(t)$, as illustrated in Fig. 1. In this figure, the blue broken line represents the widely accepted monotonically irreversible degradation path, where structural resistance either remains constant or decreases over time but never increases. On the other hand, the red broken line suggests a non-monotonic degradation path, which may initially seem improbable unless subjective factors, such as measurement and evaluation errors, are considered.

If this non-monotonic degradation path, depicted by the red broken line, can be validated through experimental methods, it would support the theoretical feasibility of modeling a Gamma process that incorporates non-monotonic resistance degradation to describe the non-stationarity of the system. This approach would offer a more accurate representation of the complex degradation behavior observed in RC components, accounting for both the accelerating and decelerating phases of the process.

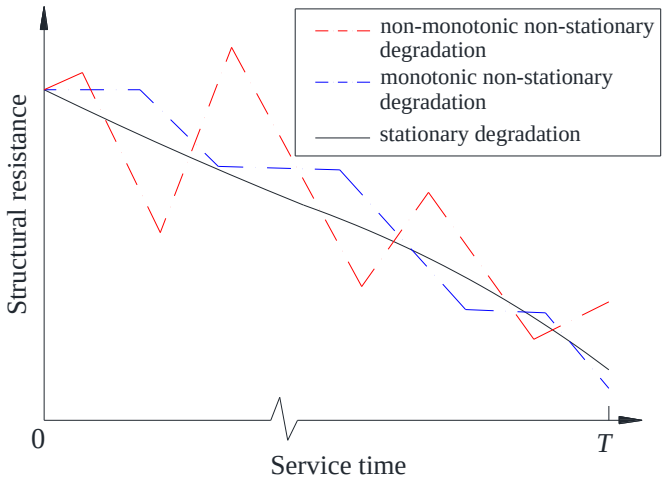

Fig. 1. Schematic illustration of non-stationary resistance degradation paths in reinforced concrete structures, comparing monotonic and non-monotonic degradation models.

Gamma process and time-dependent reliability equations are first introduced in Section 2.1 and 2.2, respectively. Then the verification based on an FE model experiment is done in Section 3.

2.1. Modelling of Gamma Degradation Process

As shown in Fig. 2, the inspected time interval $(0, T > 0]$ is divided into n sub time intervals: $(t_0, t_1], (t_1, t_2], \ldots, (t_{n-1}, t_n]$, where $t_0 = 0$, $t_n = T$, and n is a positive integer. $R(t)$ and $S(t)$ represent continuous resistance and loading processes. For each sub time intervals, R_i is the instant resistance at the end timepoint t_i for $i = 1, 2, \ldots, n$, and S_i correspondents to the instant maximum load intensity of the i-th sub-interval $(t_{i-1}, t_i]$ with its occurrence time subjected to the uniform distribution.

The average deterioration increment of structural resistance, ΔR_i, is calculated as follows [36]:

$$\Delta R_i = R_0 \cdot \alpha_i \cdot t^{\xi} \cdot \Delta t_i \quad (1)$$

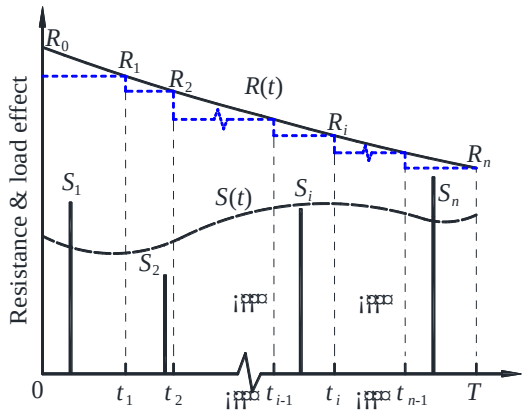

Fig. 2. Diagram of resistance degradation.

where α_i and ξ are parameters, and $\Delta t_i = t_i - t_{i-1}$. The form of Eq. (1) is derived by substituting the exponential degradation function of R(t), which is expressed as follows [41]:

$$R(t) = \begin{cases} R_0, t \le T_{ini} \\ R_0 \cdot \alpha (t - T_{ini})^{\xi}, t > T_{ini} \end{cases} \quad (2)$$

where α is the parameter indicating corrosion rate, R_0 is the initial resistance, and T_{ini} is the initial occurrence time of steel corrosion. If $T_{ini} = 0$, EqS. (1) and (2) become identical. The structural resistance deteriorates over time, i.e. $\Delta R_i \ge 0$, so ΔR_i can be directly modeled as a Gamma-distributed random variable with shape parameter α_i and scale parameter ξ [42]. This allows ΔR_i to fluctuate with different scale and shape parameters, which introduces non-stationarity in resistance degradation and enables a Gamma process to simulate the gradual accumulation of small increments [43,44] .

Assume ΔR follows a Gamma distribution, denoted as $\Delta R \sim \mathrm{Ga}(x, \alpha, \xi)$. The probability density function (PDF) of ΔR is given by:

$$f_{\Delta R}(x) = \frac{\left(\frac{x}{\xi}\right)^{\alpha-1}}{\xi \cdot \Gamma(\alpha)} \cdot e^{\left(-\frac{x}{\xi}\right)}, x \ge 0 \quad (3)$$

where $\Gamma(z)$ represents for the Gamma function, defined as $\Gamma(z) = \int_0^{\infty} \tau^{z-1} e^{-\tau} d\tau \ (\tau > 0)$. The mean μ and variance σ^2 of ΔR have the following relationship with the parameters α and ξ, respectively:

$$\begin{cases} \mu = \alpha \cdot \xi \\ \sigma^2 = \alpha \cdot \xi^2 \end{cases} \quad (4)$$

Form Eq. (4) it is evident that μ is the product of α and ξ. To align the Gamma process with k_{ga} times of the stationary process, by assuming k_{ga} as the amplification factor. Let $\alpha = \mu$ and $\Delta R \sim \mathrm{Ga}\left(x, \frac{k_{ga} \cdot \mu}{\xi}, \xi\right)$.

Suppose $\mu = 100$ and the coefficient of variation is Cov. $= \frac{\sigma}{\mu} = 0.19$, Fig.3 shows multiple PDFs of ΔR for different k_{ga} values when $\xi = 1$, and Figs.4(a) and 4(b) illustrate the PDFs for different scale parameters when $k_{ga} = 1$.

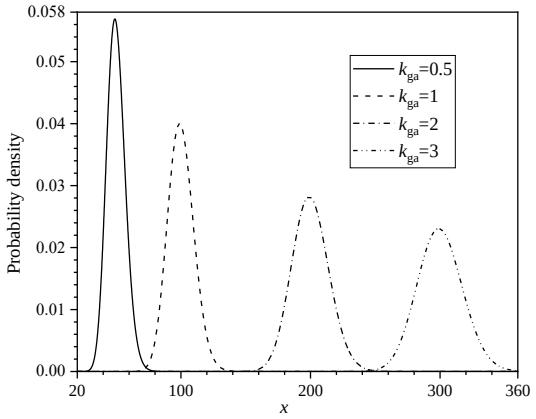

Fig. 3. PDFs of ΔR for different k_{ga} s when $\xi = 1$

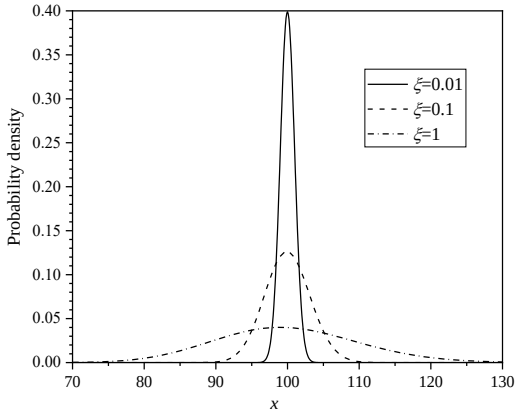

(a)

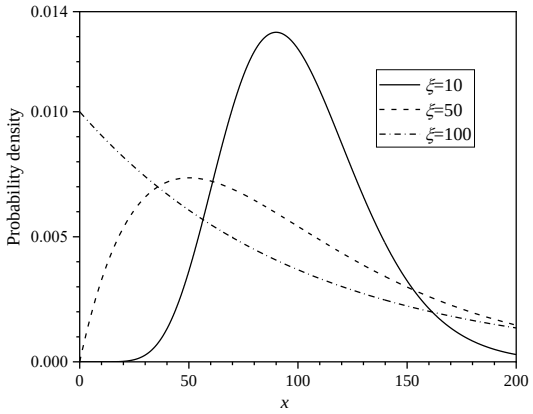

(b)

Fig. 4. PDFs of ΔR for different ξs when $k_{ga} = 1$

From Fig.3, it is observed that ΔR has the highest probability density near k_{ga} times μ. Fig. 4 shows that as the

scale parameter ξ decreases, the probability density of ΔR becomes more concentrated near μ, with a narrower fluctuation range. Conversely, as ξ increases, the probability density of ΔR spreads over a wider range. When $\xi = 100$, the density of ΔR peaks at $x = 0$. However, when ξ becomes very small, ΔR nearly degenerates into a constant, with the highest probability at μ, effectively transforming the non-stationary process into a stationary one. As ξ increases, the fluctuation range of ΔR also increases, making the non-stationarity of the process more pronounced.

By adjusting the amplification factor k_{ga}, the degree of the non-stationary process can be controlled, and the fluctuation range of ΔR can be further regulated by setting different scale parameters. This provides the theoretical basis for using the Gamma process to describe the non-stationary degradation of bridge resistance.

As shown in Fig.5, for any $i = 1,2,\dots,n-1$, the degradation increment Δ_i for $g(t)$ (5(a)), or ΔR_i for $R(t)$ (5(b)) at the ith sub interval $(t_{i-1}, t_i]$ is suggested to be a random variable that follows a Gamma distribution. Taking the degradation function $g(t)$ as an example, $\Delta_i \sim \text{Ga}\left(x, \alpha_i = \frac{k_{\text{ga}} \cdot \Delta g_i}{\xi}, \xi\right)$ where $x > 0$. The probability density function (PDF) of Δ_i is:

$$f_{\Delta_i}(x) = \frac{\left(\frac{x}{\xi}\right)^{\frac{k_{\text{ga}} \cdot \Delta g_i}{\xi} - 1}}{\xi \cdot \Gamma\left(k_{\text{ga}} \cdot \frac{\Delta g_i}{\xi}\right)} \cdot exp\left(-\frac{x}{\xi}\right), x \geq 0 \tag{5}$$

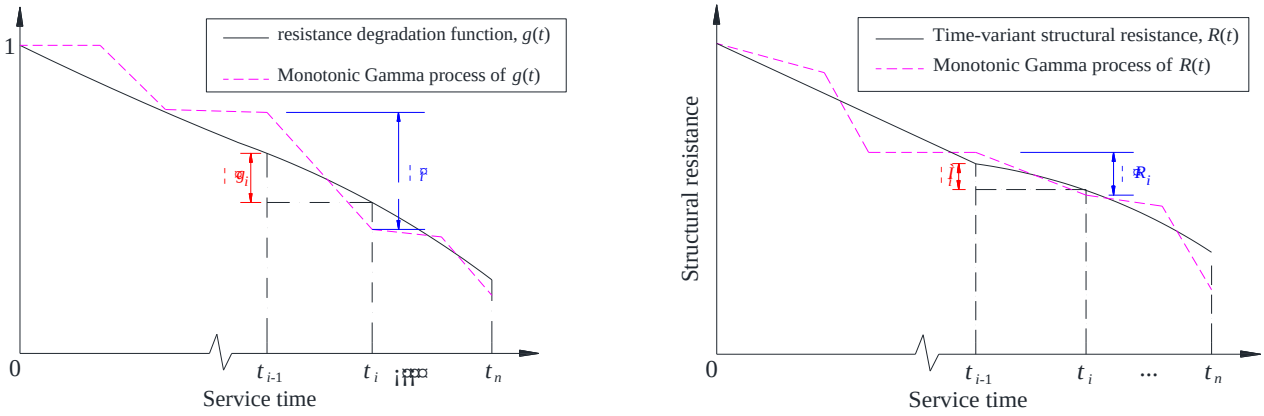

(a) (b)

Fig. 5. Sketch of Gamma random variable (Blue) and mean (Red)

where $\Delta g_i = g(t_{i-1}) - g(t_i)$.

For a monotonic Gamma process, the degrading value $g(t_i)$ at any instant point t_i can be expressed as the difference between $g(t_0)$ and the sum of previous i th random numbers $\delta_1, \delta_2, \cdots, \delta_i$ which are generated by the corresponding degradation increments $\Delta g_1, \Delta g_2, \cdots, \Delta g_i$: $g(t_i) = g(t_0) - \sum_{j=1}^{i} \delta_j$ [45].

For a non-monotonic Gamma process, assume that the degradation at each sub-interval is independent. According to the additivity property of the Gamma distribution, if $\Delta_i \sim \text{Ga}\left(x, \alpha_i = \frac{k_{\text{ga}} \cdot \Delta g_i}{\xi}, \xi\right)$, then the cumulative degrading random variable Ω_i in the previous i th total sub interval $(0, t_i]$ follows $\Omega_i \sim \text{Ga}\left(\omega, \frac{g(t_0) - k_{\text{ga}} \cdot \sum_{j=1}^{i} \Delta g_j}{\xi}, \xi\right)$, where $\omega \geq 0$.

Given this, the degradation function $g(t_i)$ can be directly expressed as: $g(t_i) = g(t_0) - \omega_i$.

The process of resistance degradation is similar that $\Delta R_i \sim \text{Ga}\left(y, \frac{k_{\text{ga}} \cdot \mu_i}{\xi}, \xi\right)$, where $y \geq 0$. The cumulative resistance degradation variable Ψ_i in the previous i-th total sub-interval $\Psi_i \sim \text{Ga}\left(\psi, \frac{R_0 - k_{\text{ga}} \sum_{j=1}^{i} \mu_j}{\xi}, \xi\right)$, where $\psi \geq 0$.

An example of the function $g(t)$ is provided here to illustrate the difference between reversible and irreversible Gamma processes. Assume that $g(t_i) = 1 - 0.01t_i$, where $t_i = i$ for $i = 1, 2, \dots, 25$. Data with fluctuation range close to $g(t)$ is selected for different values of ξ. The simulation process is shown in Fig. 6.

The result of $k_{\text{ga}} = 1$ are shown for both the irreversible and

reversible Gamma processes in Fig. 7(a) and Fig. 7(b), respectively. These figures demonstrate how the degradation paths differ between the reversible and irreversible processes under the same parameter settings, emphasizing the impact of process assumptions on the simulation outcomes.

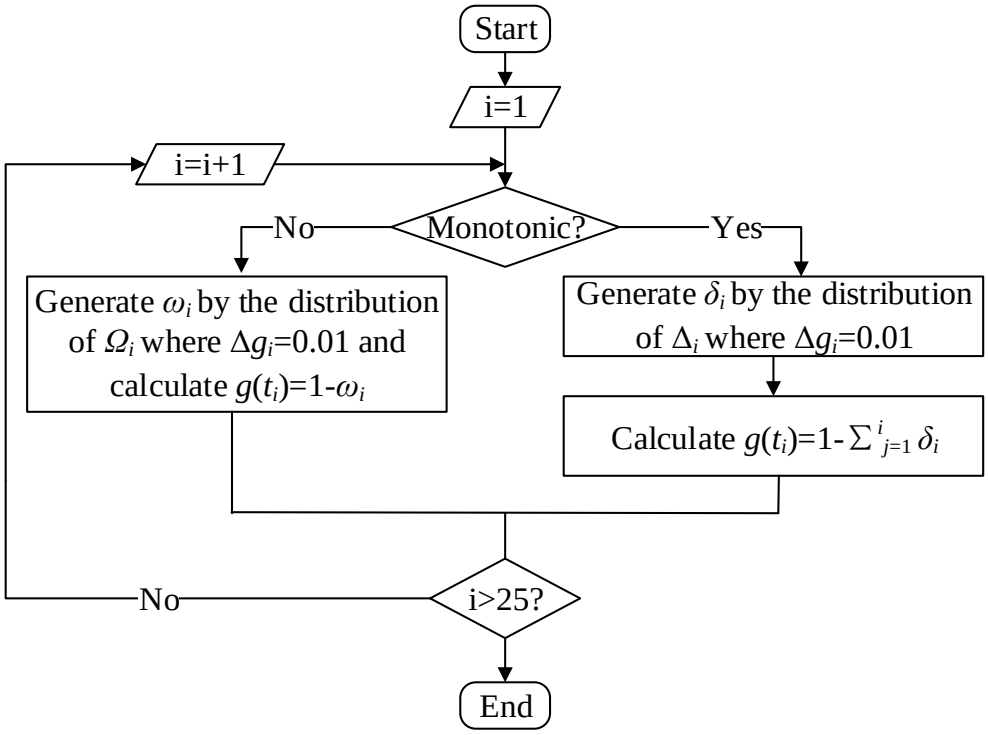

Fig. 6. Simulation procedure of Gamma process.

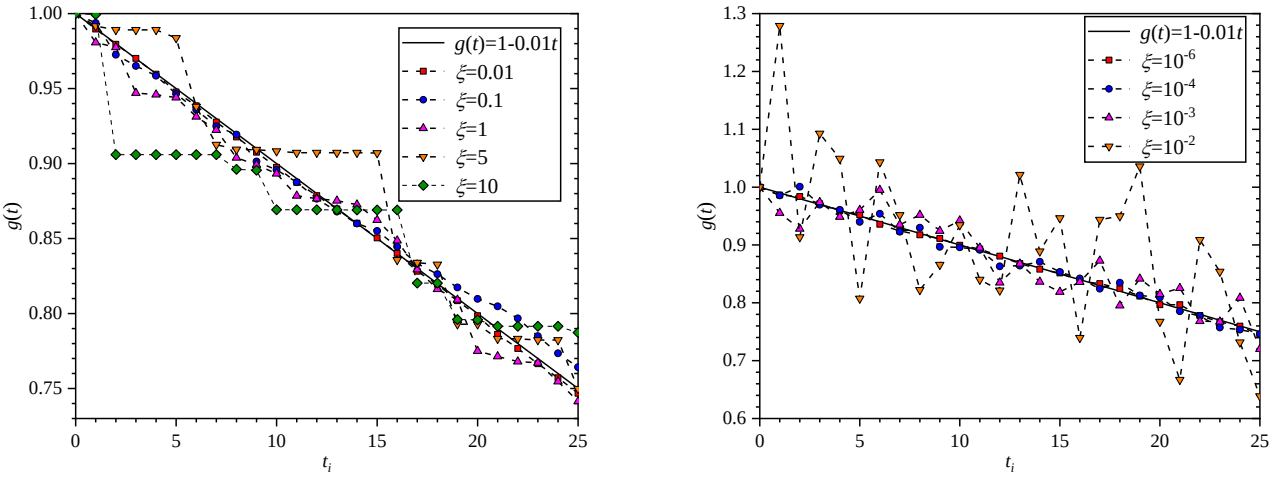

(a) (b)

Fig. 7. Monotonic (a) and non-monotonic (b) Gamma process

The non-stationary degradations shown in Fig. 6 and Fig. 7 demonstrate the feasibility of the model presented in Fig. 1. The sensitivity of the non-monotonic process is higher than that of the monotonic process concerning changes in the scale parameter, as the shape parameter of the non-monotonic process is larger.

Fig. 8 illustrates both the monotonic and non-monotonic Gamma processes when the amplification factor kga = 1, 2, and 3, respectively. The scale parameters for the non-monotonic and monotonic processes are set to 0.001 and 1, respectively. As k_{ga}, increases, both processes degrade proportionally, approaching the product of k_{ga} and $g(t)$ (represented by the dashed line in the figure). This further validates the theoretical correctness of the model depicted in Fig. 1.

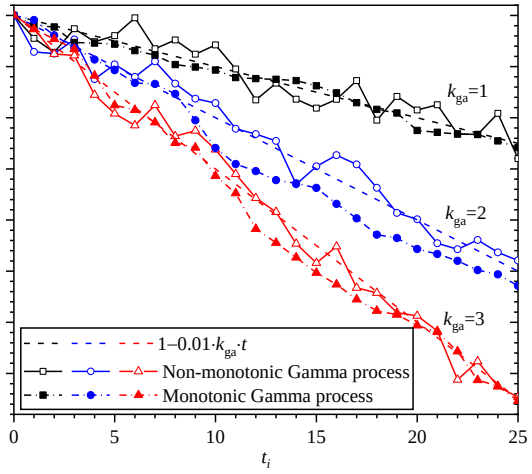

Fig. 8. Monotonic and non-monotonic Gamma processes with multiple k_{ga}s.

2.2. Time-dependent reliability analysis based on non-stationary resistance degradation

Time-dependent reliability refers to the probability that a structure remains in a safe state over a specific time interval of interest [26]. As illustrated in Fig. 2, the time interval of interest, or the inspected time interval, is $(0, T]$, and is divided by n sub intervals. The maximum load effect of each sub interval is S_1,S_2,…,S_n, with the occurrence time of each load effect uniformly distributed within the corresponding sub-interval [25]. Note that the inspected time interval does not include the initial moment t=0, since R_0 greater than the initial load, or the designed load S_0 at t=0 is considered to be an independent event and calculated saparetely as $P(R_0 > S_0)$, thereby avoiding the issue of each endpoint of the n sub intervals being included twice when dividing them.

It is assumed that the resistance value within each sub-interval equals the value at the right endpoint, resulting in a degradation pattern that appears as a 'stepped shape,' represented by the blue-dashed broken lines. If n is sufficiently large, the structural resistance within each sub-interval (which degenerates into an instant process) can be considered approximately constant

[11]. This approach simplifies the modeling of resistance degradation over time while still capturing the key elements of the process.

The time-dependent reliability in the i-th sub interval $(t_{i-1}, t_i]$ is denoted by $P_l(t_{i-1}, t_i)$, where:

$$P_l(t_{i-1}, t_i) = P(R_i > S_i) \tag{6}$$

Stipulate that when the initial point of the time interval (including sub interval) is 0, the time-dependent reliability $P_l(0, t)$ over the interval $(0, t]$ is simplified as $P_l(t)$. Besides, t_0 and t_n represent 0 and T, respectively.

Denote the cumulative distribution function (CDF) of S_i is F_{S_i}, and the accumulated increment of $g(t)$ within $(0, t_i]$ as Ω_i. The structural resistance at time t_i can then be expressed as $R_0 \cdot (1 - \Omega_i)$ where R_0 is the initial resistance.

Given this, Eq. (6) can be expressed as:

$$\begin{aligned} P_l(t_{i-1}, t_i) &= F_{S_i}(R_i) = F_{S_i}[R_0 \cdot g(t_i)] \\ &= F_{S_i}[R_0 \cdot (1 - \Omega_i)] \end{aligned} \tag{7}$$

where $g(t_0) = 1$.

Li et al. [36] assume that the structure remains reliable during its service life $(0, t]$ for any $t > 0$ and fails at T_f shortly after t, within $(t, t + \Delta t]$. Based on this assumption, they propose the structural hazard function $h(t)$ as:

$$h(t) = \frac{P(t < T_f \le t + dt)}{P(T_f > t)dt} = -\frac{\mathrm{dln}[P_l(t)]}{dt} \tag{8}$$

Once the hazard function is obtained, Eq. (8) can be transferred as [36,46,47]:

$$P_l(t) = exp\left\{-\int_0^t h(t)dt\right\} \tag{9}$$

If the initial resistance R_0 and degradation function $g(t)$ are known, the hazard function $h(t)$ can be expressed as the product of the frequency of load occurrence $\lambda(t)$, and the probability of maximum live load failure $\left[1 - F(R_0 \cdot g(t))_{S_{max}}\right]$. This represents the probability that the degraded resistance $R_0 \cdot g(t)$ is smaller than the maximum load effect $S_{\max}$ within the time interval $[0, t]$:

$$h(t) = \lambda(t)\left[1 - F(R_0 \cdot g(t))_{S_{max}}\right] \tag{10}$$

where $F(\ )_{S_{max}}$ represents the cumulative distribution function (CDF) of S_{max}. Now, substituting this expression from Eq. (10) into Eq. (9) gives:

$$P_l(t) = \exp\left\{-\int_0^t \lambda(t)\left[1 - F(R_0 g(t))_{S_{max}}\right] dt\right\} \tag{11}$$

Considering the reliability within the i-th time interval $(t_{i-1}, t_i]$ and accounting for the variability of Ω_i and R_0, let their probability density functions (PDFs) be $f_{\Omega_i}(\omega)$ and $f_{R_0}(r)$, respectively. The term $\left[1 - F(R_0 \cdot g(t))_{S_{max}}\right]$ is transferred into the variable form as $1 - F_{S_i}[r(1 - \omega)]$.

Substituting this into Eq. (11), the time-dependent reliability $P_l(t_{i-1}, t_i)$ within the interval $(t_{i-1}, t_i]$ becomes:

$$P_l(t_{i-1}, t_i) = \int_0^{\infty}\int_0^{\infty} \exp\left\{-\int_{t_{i-1}}^{t_i} \lambda_i(t)\{1 - F_{S_i}[r(1-\omega)]\}dt\right\} \cdot f_{\Omega_i}(\omega) \cdot f_{R_0}(r)drd\omega \quad (12)$$

where:

$$f_{\Omega_i}(\omega) = \frac{\left(\frac{\omega}{\xi}\right)^{\frac{k_{ga}\cdot\sum_{j=1}^{i}\Delta g_j}{\xi}-1}}{\xi \cdot \Gamma\left(\frac{k_{ga}\cdot\sum_{j=1}^{i}\Delta g_j}{\xi}\right)} \cdot e^{-\frac{\omega}{\xi}}, \omega \geq 0 \quad (13)$$

Let $\lambda_i(t)$ denote the frequency of load occurrence of the i-th sub interval. Since the reliability events at any i-th sub interval is independent, the time-dependent reliability $P_{l,T}$ within $[0, T]$ can be expressed as the product of $P(R_0 > S_0)$ and the reliabilities of the previous n sub- intervals, $P_l(T) = \prod_{i=1}^{n} P(R_i > S_i)$, as follows:

$$P_{l,T} = P(R_0 > S_0) \cdot P_l(T) = F_{S_0}(\mu_{R_0}) \cdot \prod_{i=1}^{n}\int_0^{\infty}\int_0^{\infty} \exp\left\{-\int_{t_{i-1}}^{t_i} \lambda_i(t)\{1 - F_{S_i}[r(1-\omega)]\}dt\right\} \cdot f_{\Omega_i}(\omega) \cdot f_{R_0}(r)drd\omega \quad (14)$$

If n sub intervals are not equally divided by time, the load occurrence time of the i-th sub interval is $\int_{t_{i-1}}^{t_i} \lambda_i(t)dt$, rather than $\frac{\int_0^T \lambda(t)dt}{n}$. Assume the number of total load occurrences is N. In this way N will probability not be equal to n, which is calculated as:

$$N = \left[\sum_{i=1}^{n}\int_{t_{i-1}}^{t_i} \lambda_i(t)dt\right] \quad (15)$$

To make N a natural integer, Eq. (14) can be transferred in the form of N sub intervals with unequal time length and a slightly different end time point t_N. As shown in Fig. 9, the black and blue part represent the dividing approaches of equal and unequal time length, respectively. For $j = 1,2,\ldots,N$, it guarantees that only one load S_j occurs within the j th sub interval $(t_{j-1}, t_i]$ with a time length of $\frac{1}{\int_{t_{j-1}}^{t_j} \lambda_i(t)dt}$, and a uniformly distributed occurrence time within $(t_{j-1}, t_i]$. Eq. (14) becomes:

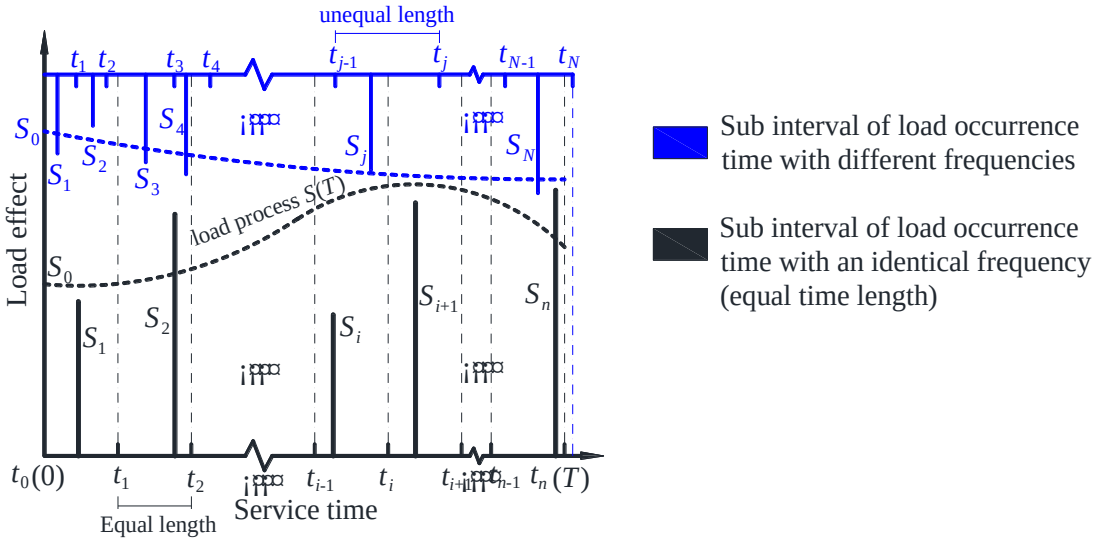

Fig. 9. Dividing approaches of equal and unequal time length.

$$P_{l,t_N} = P(R_0 > S_0) \cdot P_l(t_N) = F_{S_0}(\mu_{R_0}) \cdot \prod_{j=1}^{N}\int_0^{\infty}\int_0^{\infty} \exp\left\{-\left\{1 - F_{S_j}[r(1-\omega)]\right\}\right\} \cdot f_{\Omega_j}(\omega) \cdot f_{R_0}(r)drd\omega \quad (16)$$

where $\int_{t_{j-1}}^{t_j} \lambda_i(t)dt = 1$.

The procedure of determining t_N and N is shown in Fig. 10:

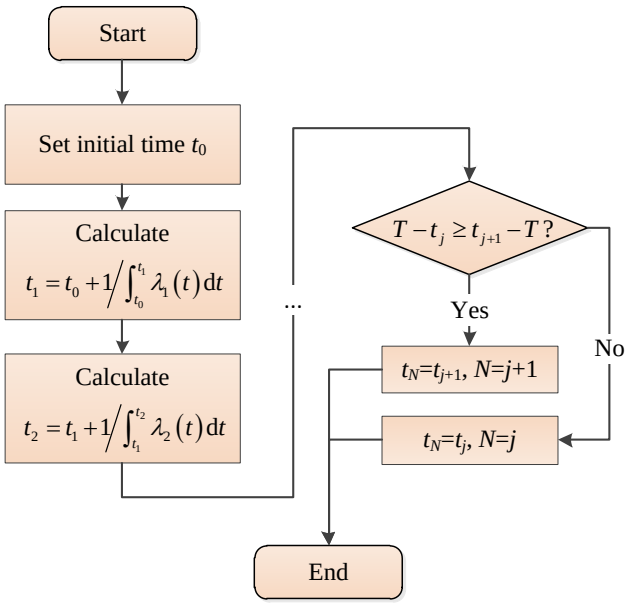

Fig. 10. Procedure of determining t_N and N.

For example, the inspected time interval is $(0,10]$, the frequency of load occurrence is $\lambda(t) = 1$ for $(0,1]$ and $\lambda(t) = 1 + 0.11t$ for $(1,9]$, N is calculated as 15.5, rounding to 16, and the sub time interval of load S_{16} is $(9.94,10.42]$. Thus, t_N and N are taken as 9.94 and 15 instead of 10 and 16, respectively, as shown in Fig. 11.

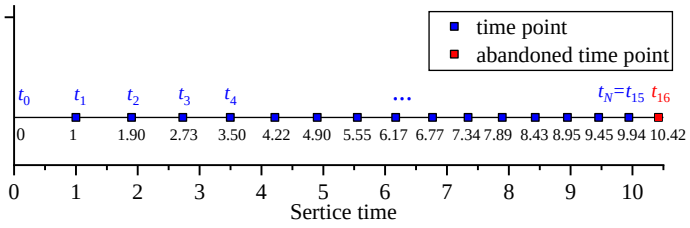

Fig. 11. Example of calculating time schedule with different frequencies of load occurrence.

There is another expression of Eq. (16) that directly incorporates resistance degradation Ψ_j within previous j th sub intervals $(0, t_j]$. The average resistance within the interval $(t_{j-1}, t_j]$ is expressed as: $R_j = R_0 - \Psi_j$, where the shape and scale parameters of the Gamma variable Ψ_j are $\frac{k_{\text{ga}} \cdot \sum_{k=1}^{j} \mu_k}{\xi}$ and ξ, respectively. Let $f_{\Psi_j}(\psi)$ be the PDF of Ψ_j. According to Eq. (16), the structural time-dependent reliability within the interval $[0, t_N]$ can be written as:

$$P_{l,t_N} = \mathrm{P}(\mathrm{R}_0 > \mathrm{S}_0) \cdot P_l(t_N) = F_{S_0}(\mu_{R_0}) \cdot \prod_{j=1}^{N} \int_0^{\infty} \int_0^{\infty} exp\left\{-\left[1 - F_{S_j}(r - \psi)\right]\right\} \cdot f_{\Psi_j}(\psi) \cdot f_{R_0}(r) dr d\psi \quad (17)$$

Accordingly, the PDF of Ψ_j for $(j = 1,2, \ldots, N)$ is expressed as:

$$f_{\Psi_j}(\psi) = \frac{\left(\frac{\psi}{\xi}\right)^{\frac{k_{\text{ga}} \cdot \sum_{k=1}^{j} \mu_k}{\xi} - 1}}{\xi \cdot \Gamma\left(\frac{k_{\text{ga}} \cdot \sum_{k=1}^{j} \mu_k}{\xi}\right)} \cdot e^{-\frac{\psi}{\xi}}, \psi \geq 0 \quad (18)$$

Eq. (16) and Eq. (17) are the time-dependent reliability equations that account for non-stationary resistance degradation based on the Gamma process. For $j = 1,2, \ldots, i$, the shape parameter of any j th increment is associated with μ_j or Δg_j and they are inconsistent with each other. The intensity of the maximum load S_j in the corresponding sub-interval $(t_{j-1}, t_j]$ can vary concerning its CDF $F_{S_j}(\ \ )$, and the variation in the frequency of load occurrence of S_i is also concerned, as N and t_N need to be calculated and determined first according to the process shown in Fig. 10.

Theoretically, Eqs. (16) and (17) are equivalent. However, since μ_i is significantly larger than Δg_i, substituting them separately into the gamma function $\Gamma(\ \ )$ can result in substantial deviations with the same scale parameter ξ, as indicated in Fig. 7. To eliminate the deviation caused by the scale parameter, the authors will only use Eq. (16) and Eq. (13), the corresponding PDF of Ω, to calculate and discuss the affections of variations of load intensity and frequency of occurrence, as well as non-stationarity of resistance degradation on the time-dependent reliability of RC bridge.

Additionally, the modeling of the Gamma distribution does not alter the properties of the RC beam, meaning that the distribution of time-variant bridge resistance remains consistent with its physical performance, associated with statistical data. Based on the first outcrossing occurrence [12,13], the time-dependent failure probability $P_f(t_N)$ is used as the failure criterion in $(0, t_N]$, denoting the structure fails if $R_j \leq S_j$ occurs for any $j = 1,2, \ldots, N$. The probability $P_f(t_{j-1}, t_j)$ denotes the failure of the structure within j-th sub interval $(t_{j-1}, t_j]$. They are shown as:

$$\begin{cases} P_f(t_N) = 1 - P_l(t_N) \\ P_f(t_{j-1}, t_j) = 1 - P_l(t_{j-1}, t_j) \end{cases} \quad (19)$$

This formulation provides a framework for assessing the failure probability over time as influenced by the stochastic nature of loads and resistance degradation.

2.3. Distribution of load effects

Among all live load effects acting on reinforced concrete (RC)

bridges, vehicle load significantly impacts bridge service life by contributing to resistance deterioration. Researchers collect accurate and comprehensive vehicle load data using tools such as the Weight-In-Motion (WIM) system, and establish extreme value extrapolation methods such as the Generalized Extreme Value (GEV) distribution, Pareto distribution, or Rice cross-threshold approach, to refine the probability density function (PDF) or cumulative distribution function (CDF) of vehicle loads [48].

Among the various types of extreme distributions, the GEV dist ribution is recommended for rationally modeling the maximum vehicle load within an inspected time interval [45,46]. The CDF of $F_{S_i}(s)$ in the form of GEV distribution of maximum load S_i at the i-th sub interval $[t_{i-1}, t_i]$ is written as:

$$F_{S_i}(s) = \begin{cases} \exp\left[-\left(1+\xi_{S_i}\cdot\left(\frac{s-u_i}{\alpha_{S_i}}\right)\right)^{-\frac{1}{\xi_{S_i}}}\right], \xi_{S_i} \neq 0 \text{ and } \xi_{S_i}\cdot\frac{s-u_i}{\alpha_i} > -1 \\ \exp\left[-\exp\left(-\frac{s-u_i}{\alpha_{S_i}}\right)\right], \xi_{S_i} = 0 \end{cases} \quad (20)$$

where u_{S_i}, α_{S_i} and ξ_{S_i} represent the location, scale and shape parameters of Si, respectively. When $\xi_{S_i} = 0$, $\xi_{S_i} < 0$ and $\xi_{S_i} > 0$, Eq. (20) converts to the CDF of Extreme type I (Gumbel) distribution, the Weibull distribution and Fréchet distribution, respectively [49].

Although the Extreme Type I distribution is not a perfectly accurate CDF for simulating load variables—since it tends to overestimate load intensity slightly and does not fully capture the sensitivity in the tail of the cumulative distribution [50], it is still a widely used probabilistic model for random load effects [11]. This is primarily because it simplifies the analysis by reducing the dimensionality of the parameter space and making it easier to obtain closed-form solutions. Therefore, this study adopts the Extreme Type I distribution to model vehicle load effects.

The location parameter u_{S_i} and scale parameter α_{S_i} of S_i have the following relationship with its mean μ_{S_i} and standard deviation σ_{S_i}:

$$\begin{cases} \alpha_{S_i} = \frac{\sqrt{6}\cdot\sigma_{S_i}}{\pi} \\ u_{S_i} = \mu_{S_i} - E_u\cdot\alpha_{S_i} \end{cases} \quad (21)$$

where Euler constant is $E_u \approx 0.577216$.

3. Verification of the Gamma process

3.1. Model description

This chapter verifies the proposed Gamma process. Fig. 12 illustrates the structure diagram of a simply supported RC beam. The beam has a span of 2.1 meters, a height of 0.2 meters, and a width of 0.12 meters, with the concrete strength classified as C30. The longitudinal tensile reinforcement consists of two HRB335 steel bars, each with a diameter of 12 mm, while the upper compression reinforcement uses two HPB235 steel bars with a diameter of 8 mm.

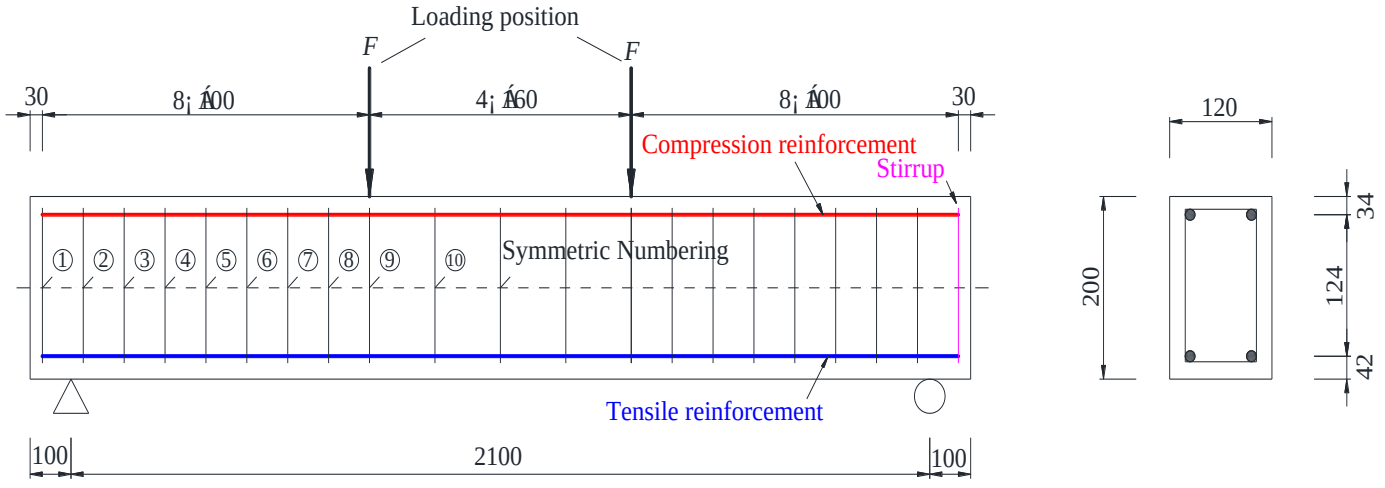

Fig. 12. Diagram of the RC beam (mm).

Additionally, 21 HPB235 steel bars, each with a diameter of 6 mm, are used as stirrups, spaced 100 mm apart on both sides and 160 mm in the middle. The thickness of the concrete protective layer is 30 mm. The loading points are positioned at 0.8 meters and 1.44 meters along the beam's length. The mechanical parameters of the steel reinforcements and concrete are provided in **Tables** 1 and 2, respectively. The slenderness ratio, shear span ratio, tensile reinforcement ratio, and stirrup reinforcement ratio of the beam are 17.5, 5.06, 0.97%, and 0.45%, respectively. This is designed for appropriately reinforced diagonal shear failure, allowing for the effective measurement of the maximum stress in the tensile reinforcement.

Table 1. Mechanical Property Parameters of Reinforcement.

Material	Tensile Strength/MPa	Modulus of Elasticity/GPa	Density kg/m^3	Poisson's Ratio
HPB235	316.5	200	7850	0.3
HRB335	455.0	210	7850	0.3

Table 2. Mechanical Property Parameters of Concrete C30.

Modulus of Elasticity/MPa	Axial compressive strength/MPa	Axial tensile strength/MPa	Co. of Crack shear trans.		Density kg/m^3	Poisson's Ratio
			Open	Close		
24000	25	2.56	0.35	0.75	2500	0.2

3.2. Modelling of the FE beam with different corrosion schemes

ANSYS is utilized to establish the finite element (FE) model of the simply supported beam. Earlier corrosion-cracking theories of reinforced concrete (RC) structures assumed that corrosion products were uniformly distributed around the surface of the steel reinforcement. Despite the occurrence of pitting corrosion, this assumption was made to simplify the analysis, leading to the development of the uniform corrosion theory [51,52]. Based on accelerated corrosion, Kashani et al. [53] employed optical surface measurement techniques to create a three-dimensional surface map of uncoated corroded steel reinforcements. The results revealed that the average depth of pitting corrosion was greater in the middle section of the steel bar than at both ends. Since the uniform corrosion assumption may overestimate the overall durability of steel reinforcement [54], two experimental schemes—one considering uniform corrosion and the other pitting corrosion—were designed.

As shown in Fig. 13, Scheme 1 uniformly reduces the overall cross-sectional area of the steel reinforcements, independent of the cracking locations; in contrast, Scheme 2 generates higher sectional loss at the mid-span and lower loss at the beam ends, dividing the reinforcement into several sections according to the relative positions of the stirrups, as shown in Fig. 12. For Scheme 2, the degree of corrosion in each section is assigned to a different amplification coefficient, k_{ga}, which adjusts the corrosion rate across different sections. The remaining cross-sectional area of each section is calculated separately, with the section loss ΔA at each section i due to corrosion is calculated as: $\Delta A = A_0 \cdot \Delta g_i \cdot k_{\mathrm{ga}}$, where A_0 is the initial cross-section of the tensile reinforcements. The corrosion of stirrups and compressing reinforcements are not considered.

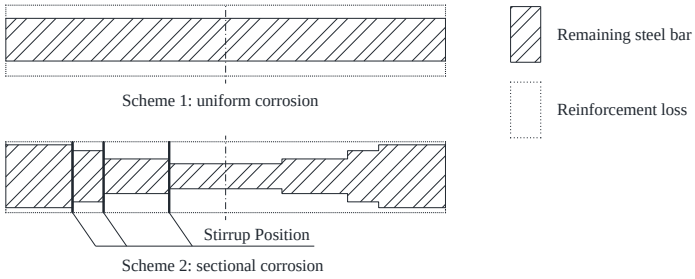

Fig. 13. Diagram of corrosion schemes.

The amplification coefficients for each section of reinforcement, $k_{\mathrm{ga}\_i,j}$ (where $j = 1,2$) in Scheme 1 and Scheme 2 are presented in **Table** 3. It is also essential to ensure that the sums of the products of the length of each section of steel reinforcement Δl_i and the correspondent amplification coefficient k_{ga_i} in both schemes are equal. This condition ensures that the total theoretical degradation values for the two

schemes are identical.

Table 3. Amplification coefficients of Reinforcement at Each Section.

Num. of Rein. i	1st. Sch.k_{ga_i1}	2nd. Sch. k_{ga_i2}	Δl_i/100mm	1 st. Scheme /$(0.01\cdot\Delta l_i\cdot k_{ga\_i1})$	2 nd. Scheme /$(0.01\cdot\Delta l_i\cdot k_{ga\_i2})$
1	1	0.6	1	1	0.6
2	1	0.7	1	1	0.7
3	1	0.8	1	1	0.8
4	1	0.9	1	1	0.9
5	1	1	1	1	1
6	1	1	1	1	1
7	1	1.1	1	1	1.1
8	1	1.1	1	1	1.1
9	1	1.2	1.6	1.6	1.92
10	1	1.3	1.6	1.6	2.08
Σ	—	—	11.2	11.2	11.2

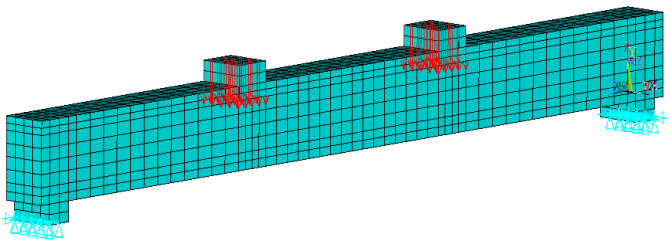

Fig. 14. FE Model of the RC beam (loaded).

The FE model of the solid beam and its reinforcement skeleton are shown in Figs. 14 and 15, respectively. Two rigid element pads simulated by Solid 185 with a density of 0 are added above the loading position to minimize the effects of stress concentration, converting the concentrated forces into pressures on the surfaces. Bonding element between the concrete and reinforcement are ignored.

The number of substeps is set to 40, with a convergence criterion of 10%. Gravitational acceleration is set at 9.8 kN · m · s^{-2}, and the minimum load increment is 0.01 kN.

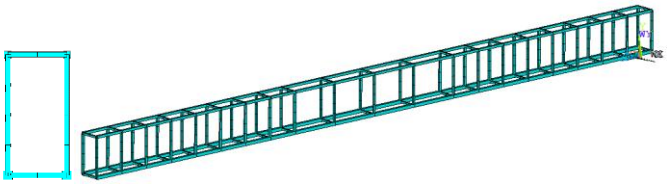

Fig. 15. Skeleton of the steel reinforcement.

For t=0 and each sub time interval $(t_{i-1},t_i]$, the ultimate load R_0 and R_i at t_i are obtained by increasing or decreasing the minimum load increment based on the principle of bracketing, respectively. The analytical approach of gathering time-variant resistance is shown in Fig. 16.

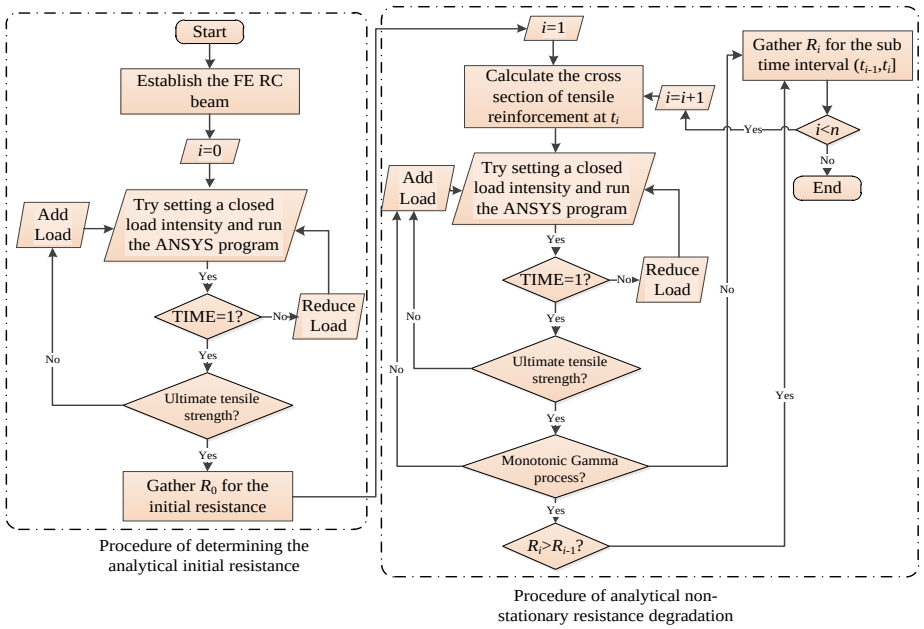

Fig. 16. Approach for gathering time-variant resistance.

3.3. Result of the Resistance Degradation

The results of the FE-model-based resistance degradation paths are displayed in Fig. 17 (a) and Fig. 17 (b). It is important to note that only one trial of each R_i for each experiment is conducted to avoid disorder. As seen in Fig. 17 (a), the resistance simulated by Scheme 1 is slightly higher than that of Scheme 2 in most years, indicating that the uniform corrosion assumption tends to overestimate the remaining resistance. However, neither scheme deviates significantly from the theoretical degradation route $R_0 \cdot g(t)$. Both schemes exhibit characteristics of the Gamma process.

In Fig. 17 (b), even without enforcing the monotonic condition that R_{i+1} must be less than R_i, the degradation still resembles a stepped, irreversible degradation path. However, there are instances where $R_{i+1}>R_i$ in the simulation results, which confirms the presence of a non-monotonic Gamma process. Consequently, the assumption illustrated in Fig. 1 and the two proposed equations are experimentally validated.

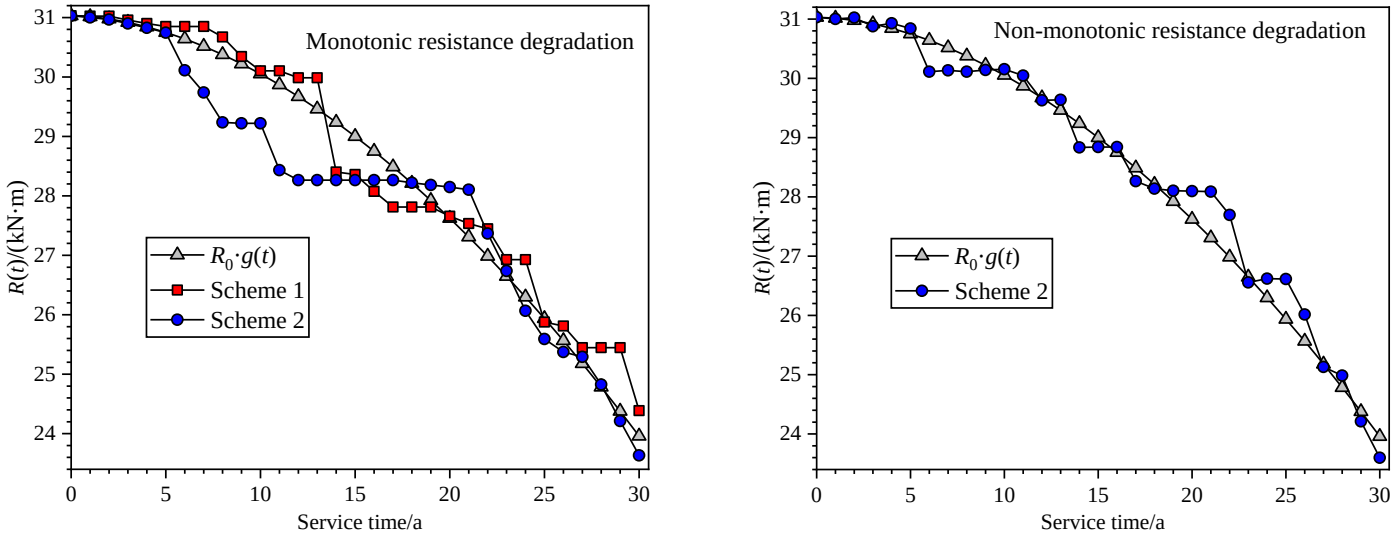

(a) (b)

Fig. 17. Time-variant resistances based on the two schemes (a) Monotonic; (b) Non-monotonic.

4. Case study

4.1. Bridge description, statistical information and parameter settings

As shown in Fig. 18, a multi-span simply supported RC beam bridge in a county road of Sichuan, China has been in normal service for several years.

Fig. 18. Overview of the RC bridge.

Each span has 5 T-shaped girders with the unique length of 20m. The strength of concrete, the longitudinal reinforcement and stirrups of the girders are C40, HRB335 and HPB300, respectively. The bridge overview is shown in Fig. 18; the cross-sectional dimension and mode of load application to the bridge are shown in Fig. 19 (a) to 19 (c), respectively.

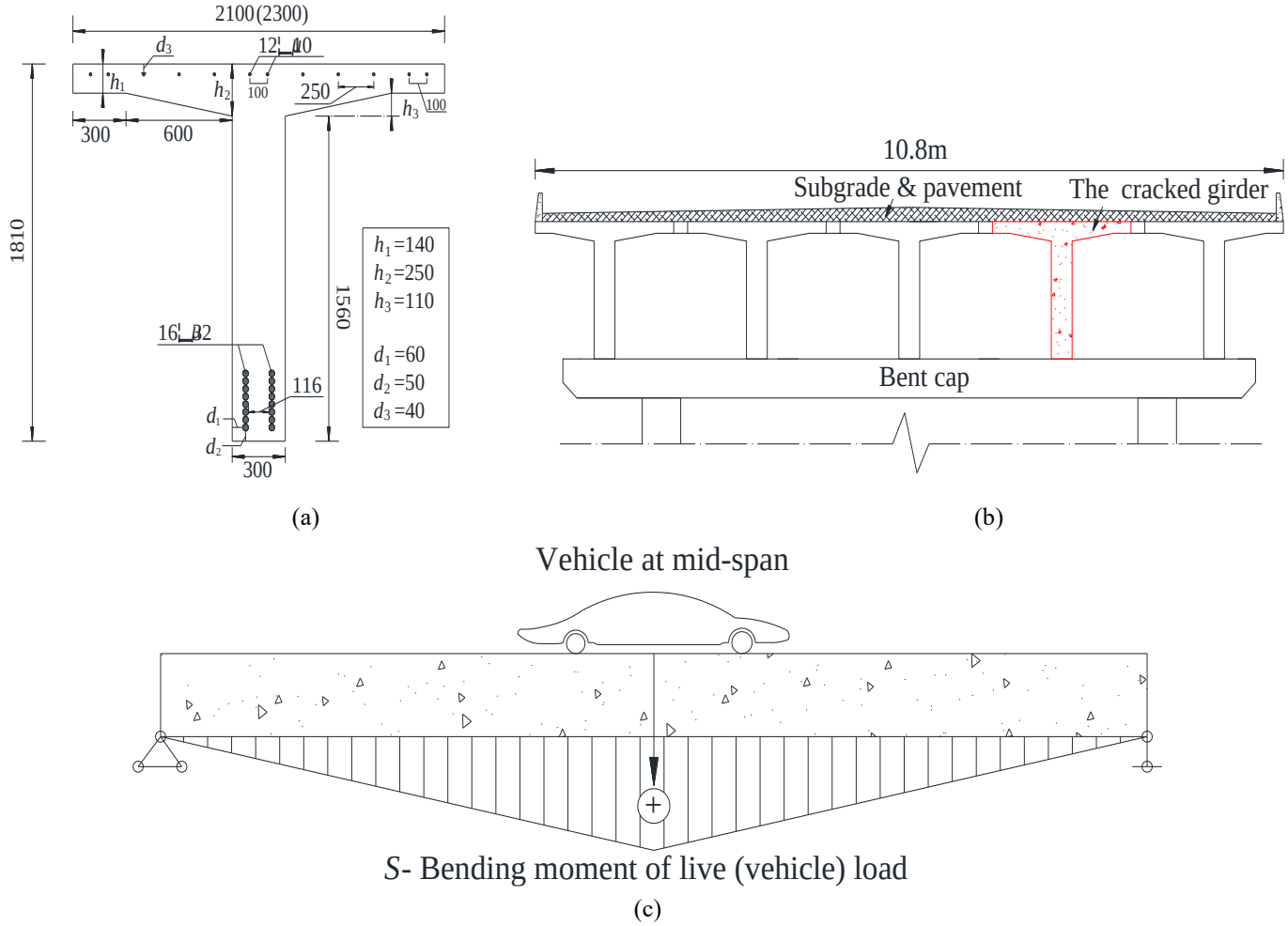

Fig. 19. Diagram of the bridge and mode of load effects (a) girder dimension; (b) cross-section and the cracked girder; (c) mode of vehicle load.

According to the Chinese standards 'General specifications for design of highway bridges and culverts (JTG D60-2015)' [55] and the 'Standards for technical condition evaluation of highway bridges (JTG/T H21-2011)' [56], the natural potential detection of the bridge indicates that all girders are functioning normally. All epoxy resin coatings on the reinforcements of girders are intact and undamaged, except for the 4th girder of the 2nd span, denoted by the red box in Fig. 18, which has some shallow, thin cracks with width less than 5mm in the tensile zone at the bottom, indicating that the corrosion has begun to happen, and the resistance of this girder will soon decline. If the first passage of vehicle load larger than resistance in this girder occurs, it brings failure to the whole bridge. On such, the time-dependent reliability of this bridge within the next 30 years is calculated using the proposed equation.

According to the 'Unified standard for reliability design of highway engineering structures (JTG 2120-2020)' [57] and 'JTG D60-2015' [55], the girder's initial resistance excluding its own weight and constant loads is calculated as $R_0 = 5800\text{kN} \cdot \text{m}$, which follows Log-normal distribution in terms of mid-span bending moment with a coefficient of variation (CoV.) 0.15 [4]. Historical load information of a nearby national highway from 2013 to 2022 indicates that the yearly maximum vehicle load, if acting on this bridge, will be 2000 $\text{kN} \cdot \text{m}$ in terms of mid-span bending moment subjected to Gumbel distribution, with an estimated CoV. 0.2, and approximate growth rate less than 3%, as well as a frequency growth rate about 3%. Enright [58] recommended an empirical degradation function as $g(t) = 1 - a(t - T_{ini})$ where a is the environment corrosion parameter. Table 4 exhibits the parameter settings with respect to scale parameter ξ of non-stationary degradation, annual load intensity growth rate ε_1, annual frequency growth rate ε_2, and the environment corrosion parameter a. The vehicle load effects are assumed to be independent, and the amplification coefficient k_{ga} is set 1. The MCS method is used for numerical verification of the Cases marked in red.

Table 4. Parameter settings.

Case Num.	Scale parameter ξ	Environmental parameter a	Lontensity growth rate ε_1 /%	Frequency growth rate ε_2 /%	Note
1	0.005	0.005	0	3	Cont. group
2	0.008	0.005	0	3	Compare the affection of the non-stationarity of bridge resistance degradation
3	0.01	0.005	0	3	
4	0.02	0.005	0	3	
5	0.04	0.005	0	3	
6	0.06	0.005	0	3	
7	0.08	0.005	0	3	
8	0.1	0.005	0	3	
9	0.005	0.001	0	3	Compare the affection of Environmental factors with respect to corrosion rate of reinforcements
10	0.005	0.002	0	3	
11	0.005	0.003	0	3	
12	0.005	0.004	0	3	
13	0.005	0.006	0	3	
14	0.005	0.007	0	3	
15	0.005	0.008	0	3	
16	0.005	0.009	0	3	
17	0.005	0.01	0	3	
18	0.005	0.005	0.5	3	Compare the affection of load intensity growth
19	0.005	0.005	1	3	
20	0.005	0.005	1.5	3	
21	0.005	0.005	2	3	
22	0.005	0.005	2.5	3	
23	0.005	0.005	3	3	
24	0.005	0.005	0	0	Compare the affection of frequency growth of load occurrence
25	0.005	0.005	0	2	
26	0.005	0.005	0	4	
27	0.005	0.005	0	6	
28	0.005	0.005	0	8	
29	0.005	0.005	0	10	
30	0.005	0.005	0	20	

4.2. Results evaluation

MATLAB R2016a is used to program calculations as well as MCSs. The first passage probability, or the time-dependent failure probability of Cases 1-8, 9-17, 18-23 and 24-30 are shown in Fig. 20 to Fig. 23, respectively. According to the fact, since corrosion has begun in the cracked girder, set current time the initial time point t=0 with T_{ini}=0, and $P(R_0 - S_0 > 0) = 1$.

Fig. 20 illustrates the time-dependent failure probability with the change of different scale parameters. For the cases where ε_2 equals 3%, the start and end point of each sub time interval of load occurrence is shown in Table 5, where N and t_N equals 44 and 30.4338, respectively.

Table 5. Start and end point of each sub interval

j	t_j	j	t_j	j	t_j	j	t_j	j	t_j
1	1	10	8.9252	19	15.5613	28	21.3883	37	26.6461
2	1.9709	11	9.714	20	16.243	29	21.9975	38	27.2019
3	2.915	12	10.4883	21	16.9154	30	22.5999	39	27.7525
4	3.8346	13	11.249	22	17.5788	31	23.1959	40	28.2982
5	4.7315	14	11.9967	23	18.2335	32	23.7855	41	28.839
6	5.6072	15	12.732	24	18.8799	33	24.3691	42	29.3752
7	6.4632	16	13.4556	25	19.5183	34	24.9468	43	29.9067
8	7.3008	17	14.168	26	20.149	35	25.5187	44	30.4338
9	8.1211	18	14.8698	27	20.7723	36	26.0851		

According to the judgment criteria of Fig. 10, the calculation should be terminated at j=43. Due to the proximity of t_{44} to the endpoint of the interval, 30, the author still calculated the results for t_{44}. From Fig. 20, it is seen that the non-stationarity of resistance deterioration indeed increases the probability of failure of the structure. Specifically, $P_f(1)$ and $P_f(30.4338)$ are 0.0009 and 0.0683, respectively, which is an increase of 75.9 times, showing a significant change. Additionally, for the three cases where ξ>0.04, some numerical solutions close to the beginning of the sub intervals cannot be represented using the VPA command. In these cases, the failure probability results are taken from the cases with the largest ξ. As a result, the numerical results of MCS are slightly larger than those of equations when ξ increases, since equations have 'borrowed' some smaller failure probabilities from smaller scale parameters.

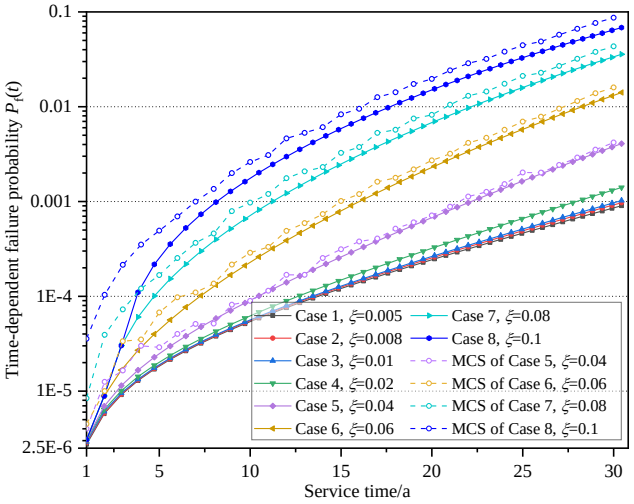

Fig. 20. Time-dependent failure probability influenced by scale parameters.

Fig. 21 shows the impact of environmental parameters on the time-dependent failure probability, where a=0.005 (the Control group) corresponds to the parameter value recommended by Enright [53] under medium corrosion environment. When a equals 0.001, 0.005, and 0.01, the first passage probabilities over the whole time period (0, 30.4338] are 0.00016, 0.0009, and 0.0102, respectively. Although they still exhibit a nonlinear growth trend, the increase in the time-dependent failure probability due to changes in environmental parameters is much slower and more moderate compared to the changes caused by the non-stationarity of resistance deterioration parameters.

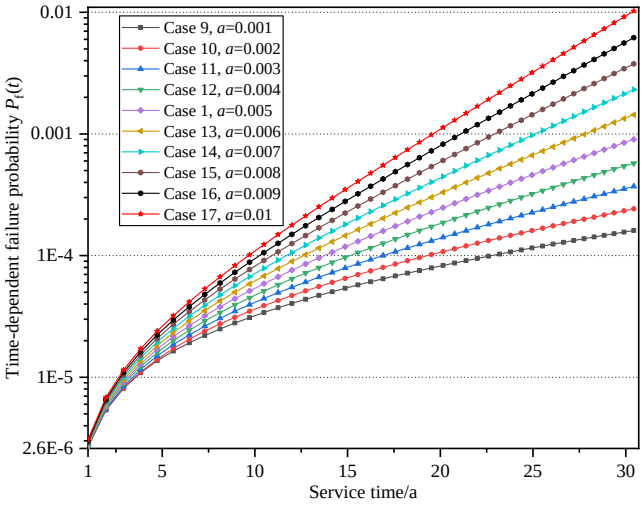

Fig. 21. Time-dependent failure probability influenced by environmental parameters.

Fig. 22 illustrates the impact of the load growth rate on the time-dependent failure probability. It can be observed that with each increase of 0.5% in ε_1, the increase of structure's time-dependent failure is highly pronounced. When ε_1 increases from 0% to 3%, the values of $P_f(30.4338)$ are 0.0009, 0.005, 0.021, 0.067, 0.167, 0.339, and 0.561, respectively. As load intensity severely affects bridge safety, during the bridge service, systems like WIM should be used for regular monitoring of vehicle loads. If the growth of load intensity is found too rapid, restrictions on heavy vehicle transit should be implemented. In addition, compared to Cases 5 to 8, the MCS results of Cases 18 and 23 are much closer to the calculated solutions, because in these two cases, the scale parameters are both 0.005, and the time-dependent reliability in the initial years does not need to 'borrow' results from smaller scale parameters.

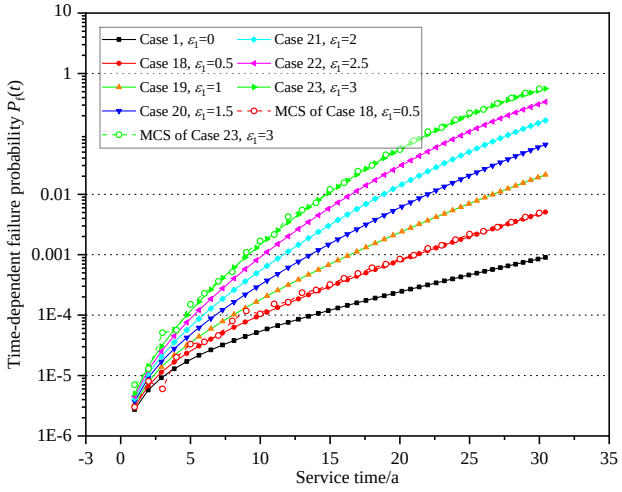

Fig. 22. Time-dependent failure probability influenced by growth rate of vehicle load

Fig. 23 presents the calculated results of the time-dependent failure probability under frequency growth. It can be seen from the figure that when the distribution parameters of the maximum load intensity S at each sub interval remain unchanged, the effect of frequency growth on the time-dependent failure probability is relatively moderate. However, when ε_2 equals 0%, 10%, and 20%, respectively, the $P_f(t_N)$ of Case 24, 29 and 30 are 0.0005, 0.0016, and 0.0027, respectively. Although the base value is small, the times of increase is still significant and should not be underestimated.

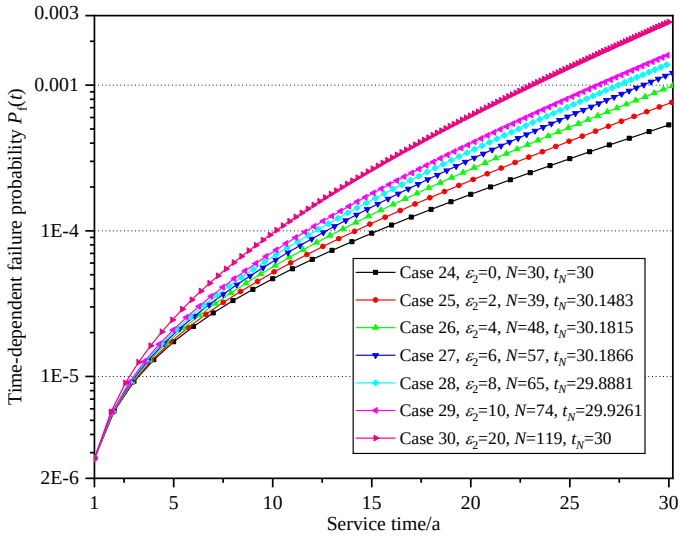

Fig. 23. Time-dependent failure probability influenced by the frequency growth of load occurrence.

In addition, the MCS results of each marked Case indicate high

4.3. MCS verification and discussion

MCS results of each Case marked red in Table 5, shown in Fig. 20 to 23 show that the numerical simulations are very close to the integral calculation results, demonstrating the correctness of the equations proposed in this paper. The procedure of simulating $P_l(T)$ is shown in Fig 24.

Noted that the right endpoint t_{j+1} of each sub-time interval is an integer equal to $j+1$. This is because N in the simulation has already been considered as a non-integral parameter of the Poisson distribution, resulting in expected outcomes. When $t \leq 10$, the number of simulations, Q for each Case is 2 million, and Q equals 1 million for $t > 10$.

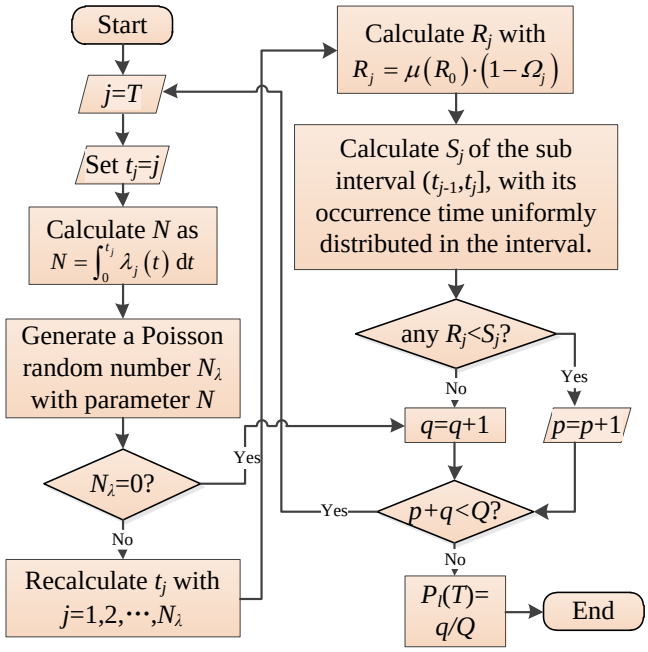

Fig. 24. Flowchart of the MCS program for simulating $P_l(T)$.

4.4. Sensitivity analysis

Based on the analysis in section 4.2, whether for the influential load growth rate or the less influential frequency growth rate, the increase in the probability of bridge foundation failure shows a geometric growth pattern. Therefore, it is necessary to use sensitivity analysis indicators to analyze the degree of influence of all parameters, by using the following equations [59]:

$$N_i = f_{max}(x_i) - f_{min}(x_i) \tag{22}$$

$$SA = \frac{N_i}{\sum_{j=1}^{n} N_j} \tag{23}$$

where: $f_{min}(x_i)$: lowest result estimated by the model; $f_{max}(x_i)$: highest result estimated by the model; and i: the range of input parameters while maintaining other variables constant. $f_{max}(x_i)$ is calculated as the highest failure probability for $(0, t_N]$ divided by the parameter difference of the correspondent group, and $f_{min}(x_i)$ is the lowest failure probability of $(0, t_N]$ divided by the parameter difference. Table 6 shows the results of SA values of each parameter, and Fig. 25 plot the ratio of their affections.

The results indicate that when measuring the same variations in influencing factors, the proportions of SA obtained from load intensity increase, non-stationary degradation of resistance, environmental parameter and frequency of load occurrence are 56.1%, 40.5%, 0.03%, and 3.37%, respectively. This demonstrates that structural reliability is most sensitive to load

intensity increase and non-stationary degradation of resistance, is relatively sensitive to corrosion rate induced by the environment, and is almost completely insensitive to the increase in load-occurrence frequency.

Table 6. SA values of each parameter.

	Scale parameter ξ	Intensity growth rate ε_1	Intensity growth rate ε_2	Environmental factor a
min $P_f(t_N)$	0.00090	0.00090	0.00053	0.00016
max $P_f(t_N)$	0.06832	0.56115	0.00271	0.01024
Para. difference	0.005	0.03	0.2	0.009
SA value	13.48	18.67	0.01	1.12

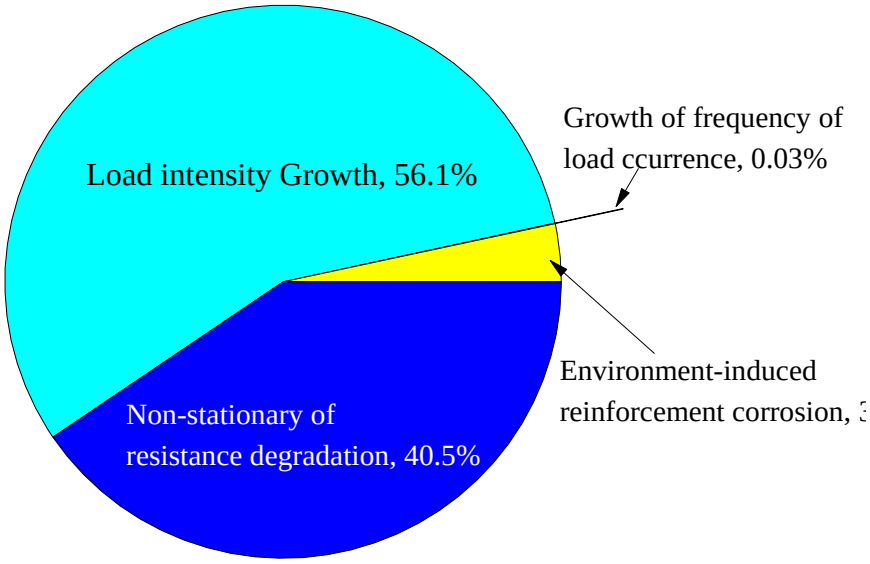

Fig. 25. Sensitivity ratio associated with parameter affections.

5. Conclusion

This study has made significant progress in understanding the reliability of RC structures as they age, offering an effective modeling approach to describe the degradation process of RC structures. Two novel time-dependent reliability equations have been developed to assess the reliability of aging structures. These equations have been validated through an FE model of a RC beam and incorporated non-stationary resistance degradation. The calculation results were verified using MCS, confirming the validity of the equations. The proposed method indicates that the assumption of uniform corrosion often overestimates time-variant resistance, and the non-stationary degradation characteristics of bridge resistance indeed increase the probability of structural failure during the time period of interest. The following conclusions are drawn:

- The reversible Gamma process is suitable for simulating the non-stationary degradation of RC structures. The overall degradation path of the FE beam more closely resembles a monotonic process. Interestingly, the degradation differences between the two schemes confirm that the assumption of uniform corrosion overestimates the time-varying resistance of the structure.
- The proposed approach is more effective for modeling non-stationary resistance degradation, as it accounts for the subjective errors in engineering measurements, a factor verified by the FE experiment. Additionally, by setting $\xi_{S_i} \neq 0$, the distribution of Si shifts to other types of GEV distributions, which allows for the examination of the impact of load variable non-stationarity.
- It is unexpectedly observed that the time-dependent failure probability of the structure is highly sensitive to non-stationary degradation of resistance, occupying 40.5%, comparable to its sensitivity to the load intensity growth, 56.1%. This indicates that the non-stationarity of resistance degradation may be a more significant issue that warrants further attention because we set k_{ga}=1, meaning that its expectation does not increase over time, unlike load intensity or time of

occurrence with growth trend.

- Sensitivity analysis reveals that the increase in load intensity and non-stationary resistance degradation are the primary risk factors for bridge failure. These two factors account for nearly 97% of the sensitivity effect on the time-dependent failure probability during the inspected time interval. Compared to an increase in load frequency at the same rate, the increase in load intensity could raise the failure probability by several hundred times within 30 years. The risk posed by traffic congestion, in the absence of a corresponding increase in load intensity, may not be as severe as anticipated, as it typically does not lead to a geometric increase in failure risk and is almost completely insensitive to changes in failure probability.
- The calculation method proposed in this study can yield a range of time-dependent reliability estimates based on subjective judgments of the structure's remaining service life in relation to time-varying resistance. This provides civil engineers with a reference for estimating structural safety under varying degrees of resistance degradation.

The study acknowledges several limitations that need to be addressed in future research.

- First, the influence and sensitivity of non-stationarity ($\xi_{S_i} \neq 0$) and the time-related correlativity of load effects on bridge reliability were not discussed. This gap leaves room for further exploration to understand how these factors impact the reliability of aging structures.
- Second, the analysis assumes that the strength and physical properties of steel reinforcements and concrete remain unchanged over time (e.g., stiffness). This assumption disregards the effects of fatigue on structural components, which can significantly influence reliability. To address this issue, it is necessary to establish a reliability model for reinforced concrete (RC) structures that accounts for the time-dependent deterioration of material properties, based on fatigue experiments.
- Third, the modeling of non-stationary resistance degradation relies on the additivity of the Gamma process, implying that the degradation values ΔR_i or Δ_i at each sub-interval t_{i-1}, t_i, i=1, 2, ... ,n are independent of each other. If the correlativity among these Gamma-distributed variables is considered, the method proposed in this study may no longer be applicable. To overcome this limitation, the study recommends exploring alternative mathematical approaches, such as surrogate modeling based on Polynomial Chaos theory, in future research.

In summary, the paper identifies key limitations, including the need to incorporate non-stationary load effects, model time-dependent material deterioration, and consider the correlativity of degradation increments in the Gamma process. Addressing these limitations through future research will enhance predictions and reliability analysis for aging infrastructure, ensuring more accurate and comprehensive assessments.

Funding

This Study Was Funded by the Natural Science Foundation of China (NSFC), No. 51778532.

References

1. Y. Bai, W. Niu, G. S. Mei et al., Flexural behavior of hybrid C-PET FRP-strengthened RC beams with U-strip anchorages, Engineering Structures 322B (2025) 119164.
2. C. JIN, Y. QIAN, F. ZHANG, W. XU, Time-dependent reliability analysis of deteriorating reinforced concrete bridges considering nonstationary processes, Chinese Journal of Engineering 44 (2022) 1265–1273.
3. C. Wang, Structural reliability and time-dependent reliability, Springer, 2021. https://doi.org/10.1007/978-3-030-62505-4
4. C. Jin, J. Huang, Y. Qian, W. Xu, Time-dependent reliability analysis for in-service bridge considering correlated non-stationary stochastic process, 2021. https://doi.org/10.1109/ISTTCA53489.2021.9654627.
5. Y. Yang, J. Peng, C.S. Cai, Y. Zhou, L. Wang, J. Zhang, Time-dependent reliability assessment of aging structures considering stochastic resistance degradation process, Reliab Eng Syst Saf 217 (2022) 108105.

6. R.K. Biswas, M. Iwanami, N. Chijiwa, K. Nakayama, Numerical evaluation on the effect of steel bar corrosion on the cyclic behaviour of RC bridge piers, Mater Today Proc 44 (2021) 2393–2398. https://doi.org/10.1016/j.matpr.2020.12.453
7. B. Nie, S. Xu, Y. Wang, Time-dependent reliability analysis of corroded steel beam, KSCE Journal of Civil Engineering 24 (2020) 255–265. https://doi.org/10.1007/s12205-020-1478-z
8. L. Luo, X. Xie, Y. Zhang, W. He, Overview of Calculation Methods of Structural Time-Dependent Reliability, J Phys Conf Ser 2148 (2022) 012063. https://doi.org/10.1088/1742-6596/2148/1/012063.
9. C. Song, C. Zhang, A. Shafieezadeh, R. Xiao, Value of information analysis in non-stationary stochastic decision environments: A reliability-assisted POMDP approach, Reliab Eng Syst Saf 217 (2022) 108034.
10. S. Wang, L. Zhang, H. Su, J. Du, Time-dependent robustness-based condition assessment of RC bridges subjected to corrosion, in: Structures, Elsevier, 2021: pp. 4500–4510. https://doi.org/10.1016/j.istruc.2021.10.061
11. C. Wang, Estimation of time-dependent reliability of aging structures under correlated load and autocorrelation in resistance deterioration, Appl Math Model 94 (2021) 272–284. https://doi.org/10.1016/j.apm.2021.01.033
12. K.J. Stein, Â.G. Graeff, M.R. Garcez, Structural performance of reinforced concrete beams subjected to combined effects of corrosion and cyclic loading, Journal of Building Pathology and Rehabilitation 8 (2023) 15. https://doi.org/10.1007/s41024-022-00263-1
13. Y. Luo, H. Zheng, H. Zhang, Y. Liu, Fatigue reliability evaluation of aging prestressed concrete bridge accounting for stochastic traffic loading and resistance degradation, Advances in Structural Engineering 24 (2021) 3021–3029. https://doi.org/10.1177/13694332211017995
14. Y. Ma, Z. Guo, L. Wang, J. Zhang, Probabilistic life prediction for reinforced concrete structures subjected to seasonal corrosion-fatigue damage, Journal of Structural Engineering 146 (2020) , https://doi.org/10.1061/(ASCE)ST.1943-541X.0002666
15. C. Wang, M. Beer, B.M. Ayyub, Time-dependent reliability of aging structures: Overview of assessment methods, ASCE ASME J Risk Uncertain Eng Syst A Civ Eng 7 (2021). https://doi.org/10.1061/AJRUA6.0001176
16. J. Zhong, Y. Mao, X. Yuan, Lifetime seismic risk assessment of bridges with construction and aging considerations, in: Structures, Elsevier, 2023: pp. 2259–2272. https://doi.org/10.1016/j.istruc.2022.12.035
17. B. Wu, Y. Tang, Z. Li, K. Tang, Fatigue damage accumulation modelling of critical components subjected to moving crane loads in reinforced-concrete industrial buildings, Eng Fail Anal 119 (2021) 104951.
18. D.K. Devendiran, S. Banerjee, Influence of combined corrosion–fatigue deterioration on life-cycle resilience of RC bridges, Journal of Bridge Engineering 28 (2023) https://doi.org/10.1061/JBENF2.BEENG-5708
19. C. Wang, Structural reliability and time-dependent reliability, Springer, 2021. https://doi.org/10.1007/978-3-030-62505-4
20. F. Matteo, G. Carlo, P. Federico, Z. Enrico, Time-dependent reliability analysis of the reactor building of a nuclear power plant for accounting of its aging and degradation, Reliab Eng Syst Saf 205 (2021) 107173.
21. L. Capacci, F. Biondini, Probabilistic life-cycle seismic resilience assessment of aging bridge networks considering infrastructure upgrading, Structure and Infrastructure Engineering 16 (2020) 659–675. https://doi.org/10.1080/15732479.2020.1716258
22. M.E.A. Ben Seghier, B. Keshtegar, H. Mahmoud, Time-dependent reliability analysis of reinforced concrete beams subjected to uniform and pitting corrosion and brittle fracture, Materials 14 (2021) https://doi.org/10.3390/ma14081820
23. C. Wang, Structural reliability and time-dependent reliability, Springer, 2021. https://doi.org/10.1007/978-3-030-62505-4
24. B.R. Ellingwood, Y. Mori, Probabilistic methods for condition assessment and life prediction of concrete structures in nuclear power plants, Nuclear Engineering and Design 142 (1993) 155–166. https://doi.org/10.1016/0029-5493(93)90199-J
25. Y. Mori, B.R. Ellingwood, Reliability-based service-life assessment of aging concrete structures, Journal of Structural Engineering 119 (1993) 1600–1621. https://doi.org/10.1061/(ASCE)0733-9445(1993)119:5(1600)
26. Y. Ji, H. Liu, N.-C. Xiao, H. Zhan, An efficient method for time-dependent reliability problems with high-dimensional outputs based on adaptive dimension reduction strategy and surrogate model, Eng Struct 276 (2023) 115393.
27. J.M. Van Noortwijk, M.D. Pandey, A stochastic deterioration process for time-dependent reliability analysis, in: Reliability and Optimization of Structural Systems, CRC Press, 2020: pp. 259–265. https://doi.org/10.1201/9781003078876-32
28. J.M. Noortwijk, A survey of the application of gamma processes in maintenance, Reliability Engineering and System Safety 94 (2009) 2-21. https://doi.org/10.1016/j.ress.2007.03.019

29. M. Oumouni, F. Schoefs, B. Castanier, Modeling time and spatial variability of degradation through gamma processes for structural reliability assessment, Structural Safety 76(2019) 162-173. https://doi.org/10.1016/j.strusafe.2018.09.003
30. D. Kuzio, R. Zimroz, A. Wyłomańska. A modified gamma process for RUL prediction based on data with time-varying heavy-tailed distribution, Information Sciences 690(2025) 121603.
31. J.M. van Noortwijk, A survey of the application of gamma processes in maintenance, Reliab Eng Syst Saf 94 (2009) 2–21. https://doi.org/https://doi.org/10.1016/j.ress.2007.03.019.
32. G. Liu, Q. Guan, Y. Tang, Y. Tzeng, Interval modeling for gamma process degradation model, Symmetry (Basel) 14 (2022) https://doi.org/10.3390/sym14050954.
33. X. Wang, B.X. Wang, Y. Hong, P.H. Jiang, Degradation data analysis based on gamma process with random effects, Eur J Oper Res 292 (2021) 1200–1208. https://doi.org/https://doi.org/10.1016/j.ejor.2020.11.036.
34. M.B. Salem, M. Fouladirad, E. Deloux, Variance Gamma process as degradation model for prognosis and imperfect maintenance of centrifugal pumps, Reliab Eng Syst Saf 223 (2022) 108417.
35. J.M. Van Noortwijk, M.D. Pandey, A stochastic deterioration process for time-dependent reliability analysis, in: Reliability and Optimization of Structural Systems, CRC Press, 2020: pp. 259–265. https://doi.org/10.1201/9781003078876-32
36. Q. Li, C. Wang, B.R. Ellingwood, Time-dependent reliability of aging structures in the presence of non-stationary loads and degradation, Structural Safety 52 (2015) 132–141. https://doi.org/10.1016/j.strusafe.2014.10.003
37. D. Jia, Z. Wu, Structural reliability analysis under stochastic seismic excitations and multidimensional limit state based on gamma mixture model and copula function, Probabilistic Engineering Mechanics 76 (2024) 103621.
38. B. Wu, L. Cui, J. Yin, Reliability and maintenance of systems subject to Gamma degradation and shocks in dynamic environments, Applied Mathematical Modelling 96(2021) 367-381. https://doi.org/10.1016/j.apm.2021.03.009
39. Q. Liang, S. Liu, C. Peng, Reliability analysis of multi-component systems subjected to dependent degradation processes and random shocks in dynamic environments, Process Safety and Environmental Protection, 190A (2024) 1546-1561. https://doi.org/10.1016/j.psep.2024.08.015
40. X. He, G. Tan, W. Chu, W. Wang, Q. Kong, Time-Dependent Reliability Assessment Method for RC Simply Supported T-Beam Bridges Based on Lateral Load Distribution Influenced by Reinforcement Corrosion, Applied Sciences 12 (2022) 7028. https://doi.org/10.3390/app12147028.
41. M.P. Enright, D.M. Frangopol, Probabilistic analysis of resistance degradation of reinforced concrete bridge beams under corrosion, Eng Struct 20 (1998) 960–971. https://doi.org/10.1016/S0141-0296(97)00190-9
42. C. Wang, An explicit compound Poisson process-based shock deterioration model for reliability assessment of aging structures, Journal of Traffic and Transportation Engineering (English Edition) 9 (2022) 461–472. https://doi.org/10.1016/j.jtte.2020.03.005
43. Y. Yuan, W. Han, G. Li, Q. Guo, X. Xu, J. Sun, Probabilistic limit state assessment of concrete bridges considering non-stationary factors, Engineering Mechanics 37 (2020) 167–178.
44. C.M. Fang Wei ZHANG Rui XIE Li, Time-varying Gamma stochastic process-based modeling method for steel corrosion, Journal Of Building Structures 41 (2020) 382–388. https://doi.org/10.14006/j.jzjgxb.2020.S2.0042.
45. C. Wang, B.M. Ayyub, A. Ahmed, Time-dependent reliability and resilience of aging structures exposed to multiple hazards in a changing environment, Resilient Cities and Structures 1 (2022) 40–51. https://doi.org/10.1016/j.rcns.2022.10.001
46. Y. Yuan, W. Han, G. Li, Q. Xie, Q. Guo, Time-dependent reliability assessment of existing concrete bridges including non-stationary vehicle load and resistance processes, Eng Struct 197 (2019) 109426.
47. J. Li, J. Chen, X. Zhang, Time-dependent reliability analysis of deteriorating structures based on phase-type distributions, IEEE Trans Reliab 69 (2019) 545–557. https://doi.org/10.1109/TR.2019.2907307
48. N. Lu, Y. Liu, M. Noori, Extrapolation of time-variant extreme effect on long-span bridge considering steadily growing traffic volume, 工程力学 35 (2018) 159–166.
49. B. Dai, D. Wu, Q. Li, Investigation of multiple-presence factor for traffic loads on road-rail bridges based on a novel extreme value analysis approach, Structural Safety 96 (2022) 102199. https://doi.org/10.1016/j.strusafe.2022.102199.
50. Z. Li, C. Li, J. Sun, Q. Li, Estimation of extreme vehicle load effect based on GPD model, Engineering Mechanics 29 (2012) 166–171.

51. Y. Liu, Modeling the time-to corrosion cracking of the cover concrete in chloride contaminated reinforced concrete structures, (1996).
52. C. Jiang, X. Zhang, P. Lun, S.A. Memon, Q. Luo, H. Sun, W. Wang, X. Wang, X. Wang, Quantitative characterization of reinforcement cross-sectional roughness and prediction of cover cracking based on machine learning under the influence of pitting corrosion, Measurement 220 (2023) 113322.
53. M.M. Kashani, A.J. Crewe, N.A. Alexander, Use of a 3D optical measurement technique for stochastic corrosion pattern analysis of reinforcing bars subjected to accelerated corrosion, Corros Sci 73 (2013) 208–221. https://doi.org/10.1016/j.corsci.2013.03.037
54. Z. Zhao, L. Fu, The probability distribution of pitting for accelerated corrosion reinforcement, Case Studies in Construction Materials 9 (2018) e00193.
55. CCDI, JTG D60-2015 General specifications for design of highway bridges and culverts, China Communication Press (2015).
56. RIHMT, JTG/T H21-2011 Standards for technical condition evaluation of highway bridges, China Communication Press (2011).
57. CCCC, JTG 2120-2020 Unified standard for reliability design of highway engineering structures, China Communication Press (2020).
58. M.P. Enright, D.M. Frangopol, Service-life prediction of deteriorating concrete bridges, Journal of Structural Engineering 124 (1998) 309–317. https://doi.org/10.1061/(ASCE)0733-9445(1998)124:3(309)
59. C. Jin, Y. Qian, S.A. Khan, et al, Investigating the feasibility of genetic algorithms in predicting the properties of ecofriendly alkali-based concrete, Construction and Building Materials, 409 (2023) https://doi.org/10.1016/j.conbuildmat.2023.134101.

Nomenclature

Abbreviations

Identifier	Description	Identifier	Description
CDF	Cumulative distribution function	NPP	Nuclear Power Plant
FE	Finite Element	PC	Prestressed concrete
FEM	Finite Element Model	PDF	Probability Density Function
GEV	Generalized Extreme Value	PDFM	Probability Density Function-Informed Method
HRB335	Hot Rolled Bar (Steel Grade)	PRA	Probabilistic Risk Assessment
HPB235	Hot Rolled Plain Bar (Steel Grade)	RC	Reinforced Concrete
JTG	Chinese Unified Standard for Reliability Design of Highway Engineering Structures (JTG 2120-2020)	TCM	Three-term conjugate map
LERF	Large Early Release Frequency	WIM	Weight-In-Motion System
MCS	Monte Carlo Simulation		

Symbols

a, b	Parameters for degradation function	Q	Number of experimental trials
E_u	Euler constant	p	Number of failure outcomes
$F(\ )_{S_{max}}$	Cumulative distribution function of S_{max}	R	Resistance
g(t)	Degradation function over time	S	Load
$h(t)$	Hazard function	T	Time interval
k_{ga}	Amplification coefficient	u_S	Location parameter
P_l(t)	Time-dependent reliability in (0,t]		
P_l(ti,tj)	Time-dep. r. in (ti,tj] for ti>0	λ(t)	Load frequency function
$P_{l,t}$	Time-dep. r. in [0,t]		
q	Number of succeed simulations	ε_S	Annual growth rate of load intensity

Subscripts and superscripts

0	Initial condition	Maximum	Maximum value
i	Index for positions or iterations	m	Refers to starting time
ini	Initial occurrence	n	Index for number
j	Sub-interval index in degradation modeling	S	Related to load effect

Greek symbols

Δ	Change or difference	Ω	Variable in Gamma distribution for degradation over time
Γ	Gamma function	ψ	Cumulative resistance degradation variable
δ	Random number	σ^2	Variance value
α	Shape parameter	λ	Load frequency

Nomenclature

Abbreviations

Identifier	Description	Identifier	Description
CDF	Cumulative distribution function	NPP	Nuclear Power Plant
γ	Coefficient used in degradation modeling	σ_S	Standard deviation of load effect
ξ	Scale parameter	ε	Annual growth rate of load frequency
μ	Mean value		